Fuel Processing Technology 267 (2025) 108173

Contents lists available at ScienceDirect

Fuel Processing Technology

journal homepage: www.elsevier.com/locate/fuproc

Repurposing of propane oxidative-dehydrogenation catalysts to deoxygenation of vegetable oils for green diesel production

S. Lucantonio [a], G. Di Vito Nolfi [b], C. Courson [c], K. Gallucci [a], A. Di Giuliano [a,c,*], L. Rossi [b]

[a] Department of Industrial and Information Engineering and Economics, University of L'Aquila, Piazzale E. Pontieri 1, 67100 L'Aquila, Italy
[b] Department of Physical and Chemical Sciences, University of L'Aquila, Via Vetoio, Coppito, 67100 L'Aquila, Italy
[c] Institut of Chemistry and Process for Energy, Environment and Health, CNRS UMR 7515 - University of Strasbourg, 25 rue Becquerel, 67087, Strasbourg Cedex 2, France

ARTICLE INFO

Keywords:
Green diesel
Catalytic deoxygenation
Biomass
Vegetable oils
Heterogeneous catalysis
Ni Zn Co Mo

ABSTRACT

The market for diesel fuel will grow in the next years. Green diesel – alkanes produced through deoxygenation (DO) with H_2 of triglyceride-based biomasses – can help cover this demand sustainably. Repurposing non-noble-metals catalysts is a faster affordable route to spread DO at larger scales. NiCoMo and ZnCoMo catalysts were previously proposed in the literature for oxidative-dehydrogenation of propane and unprecedentedly repurposed for DO in this work. DO tests on NiCoMo and ZnCoMo were performed according to an unreplicated 2^3 factorial Design of Experiment (DoE) with three replications at center point. Temperature (T), catalyst-to-oil ratio (γ), DO duration (t) were the design-factors, at levels: 280–320 °C; 4–10 $\%_{w/w}$; 2–6 h. Both catalysts performed promisingly(NiCoMo and ZnCoMo best conversion of 100 %, NiCoMo and ZnCoMo best diesel yields of 73 % and 68 %, respectively). Analysis of Variance was performed on main effects and factor interactions of all measured quantities and performance parameters, obtaining surface responses equations. Additionally, NiCoMo and ZnCoMo underwent recycling tests (four DO cycles) to evaluate reusability at 320 °C-10 $\%_{w/w}$-2 h: catalysts ensured for four cycles stable 100 % conversion of triglycerides and slightly growing diesel yield (NiCoMo: 67 % to 72 %; ZnCoMo: 64 % to 74 %). Overall, the selected dehydrogenation catalysts were successfully repurposed for DO at laboratory-scale. Although further evaluations should be performed for a balanced perspective regarding the industrial potential and sustainability of DO by repurposed NiCoMo and ZnCoMo (e.g., catalyst synthesis scalability, switch from batch to continuous production), the ease (cost-effectiveness) of the catalytic synthesis and process performances seem promising for their scalability.

1. Introduction

Since the Paris Agreement (COP21, 2015 [1]) to recent days (COP28, 2023 [2]), the shift from fossil to renewable fuels has been prioritized [3]. Proposed scenarios for the containment of global warming to +1.5 °C (with no overshoots) involve a decrease of international demands for oil, coal, and natural gas from 2020 to 2050 by 62 %, 95 %, 42 % on average, respectively [3,4].

In this traced energy transition, one cannot forget that Internal Combustion Engines (ICE) powered by fossil fuels currently represent the primary mobility option [5]; therefore, "CO_2-neutral" fuels – i.e., fuel that produces neither net greenhouse gas emissions nor a carbon footprint [5] – that work well in current ICE technologies could be a good choice to manage that transition.

Diesel engines constitute a significant share of private mobility and the preferred choice in heavy-duty [6] and sea transport [7]. The latter are critical sectors of the world economy: for instance, one can remember the inconveniencies and economic losses during the 2021 Suez Canal obstruction [8]. According to Fortune Business forecast 2024–2032 [9], the market of diesel fuel is expected to grow in the next years, e.g., because of heavy-duty and sea transport and the increase of power demand in remote zones disconnected by distribution grids (diesel power units). In addition, Europe has financed the realization of several infrastructures for alternative fuels, e.g., in the framework of the plans of ReFuelEU Aviation and FuelEU Maritime regulations [10].

Green diesel (also known as renewable diesel) is an alternative to conventional fossil diesel, with better fuel properties [11–13], and fully

* Corresponding author at: Department of Industrial and Information Engineering and Economics, University of L'Aquila, Piazzale E. Pontieri 1, 67100 L'Aquila, Italy.
E-mail address: andrea.digiuliano@univaq.it (A. Di Giuliano).

https://doi.org/10.1016/j.fuproc.2024.108173
Received 20 September 2024; Received in revised form 3 December 2024; Accepted 8 December 2024
Available online 30 December 2024

Abbreviations

AOAC	Association of Official Agricultural Chemists
ATR	Attenuated Total Reflection
BET	Brunauer-Emmett-Teller
BHC	Branched Hydrocarbons
BJH	Barrett-Joyner-Halenda
BSD	Back Scatter Detector
CCD	Central Composite Design
COP	Conference of Parties (of the United Nations Framework Convention on Climate Change)
DCO	Decarbonylation
DCO_2	Decarboxylation
DO	Deoxygenation
EU	European Union
FAME	Fatty Acid Methyl Ester
FFA	Free Fatty Acid
FT-IR	Fourier Transform Infrared Spectroscopy
GC-FID	Gas Chromatograph equipped with Flame Ionization Detector
GC–MS	Gas Chromatography-Mass Spectrometry
HDO	Hydrodeoxygenation
ICE	Internal Combustion Engine
ICP-MS	Inductively Coupled Plasma Mass Spectrometry
LDH	Layered Double Hydroxydes
ODH	Oxidative-DeHydrogenation
PSD	Particle Size Distribution
RT	Room Temperature
SBA	Santa Barbara Amorphous silica
SEM-EDS	Scanning Electron Microscopy- Energy Dispersive X-ray Spectroscopy
SM	Supporting Materials
TCD	Thermal Conductivity Detector
TG	Triglyceride
TPD	Temperature Programmed Desorption
TPR	Temperature Programmed Reduction
UHC	Unsaturated HydroCarbons
XRD	X-Ray Diffraction

List of symbols

$A\%_p$	percent of Area of component p in Agilent GC-FID chromatogram with $p = C_i$ for the n-alkane with i carbon atoms; *FAME* for unconverted oil; *UHC* for unsaturated hydrocarbons; *BHC* for branched hydrocarbons; *Others* for unidentified peaks (Eq. 5, Eq. 6, Eq. 7)
$d(x,x)$	catalysts particle diameters from PSD, $x,x = 0,1$ for 10th percentile, 0,5 for 50th percentile, 0,9 for 90th percentile, 3,2 for Sauter average particle diameter (Table S.1)
d_{BJH}	BJH averaged cylindrical pore diameter
H_0	null hypothesis in hypothesis testing
H_1	alternative hypothesis in hypothesis testing
m_{oil}	initial mass of oil fed into the reactor
$m_{product}$	mass of product recovered after the test
MS_E	pure error mean square
n_C	number of replicated observations at central point
n_F	number of unreplicated factorial observations $= 2^3$
r	number of cycle in recycling tests
S_{BET}	BET specific surface area
$S_{HDO/DCOx}$	Catalyst Selectivity
$SS_{pure\ quadratic}$	Single-degree-of-freedom sum of squares for pure quadratic curvature
t	DO duration
T	DO temperature
V_{BJH}	BJH specific pores volume
x_l	coded design variable of factor l: $-1 \le x_l \le +1$
y	generic system response in experiments
$y(lqk)$	y at generic treatment lqk
y_{jC}	j^{th} observation of y at center point ($j = 1, \ldots, n_C$)
$\overline{y}_C$	arithmetic mean of observations y_{jC}
$\overline{y}_F$	arithmetic mean of unreplicated n_F factorial observations of y
Y_{diesel}	Diesel Yield (Eq. 6)
$Y_{product}$	Product Yield (Eq. 4)
β_0	grand average of y observations
β_l	half of the main effect of factor l
β_{ll}	pure quadratic coefficient of factor l
β_{lq}	half of the interaction effect between factors l and q
γ	Catalyst-to-oil mass ratio
ε	experimental error
χ	Conversion of TGs

exploitable by current diesel ICE [12,14]. Green diesel is produced by the deoxygenation (DO) of fatty biomasses: triglycerides (TGs) react with H_2 to form linear alkanes (n-alkanes) and byproducts [13,15].

Several types of biomass have been investigated in literature for DO: animal fats (laboratory and pilot scales [16–18]); waste oils (laboratory scale [19–22]); edible and non-edible vegetable oils (laboratory, pilot and industrial scales [23–31]); microalgae (laboratory scale [32–35]). Recent concerns have emerged on the source of H_2 for biofuels production [36]: only the use of green-H_2 (e.g., photovoltaic or wind electricity powering H_2O electrolysis to form "*E*-H_2" [37]) ensures a potential of full sustainability of green diesel. In other words, green diesel is truly a CO_2-neutral fuel only if it is an E-biofuel [36].

The DO includes different reactive steps. The double bonds in acid tails of TGs are first saturated by H_2, then TGs are decomposed into C_3H_8 and free fatty acids (FFAs, R-COOH) through hydrogenolysis [38]. FFAs are converted in n-alkanes through three possible reaction pathways: hydrodeoxygenation (HDO, Eq. 1), decarbonylation (DCO, Eq. 2), and decarboxylation (DCO_2, Eq. 3) [39].

$$\textbf{HDO}: \quad R-COOH + 3H_2 \rightarrow R-CH_3 + 2H_2O \tag{1}$$

$$\textbf{DCO}: \quad R-COOH + H_2 \rightarrow R^{\cdot} - H + CO + H_2O \tag{2}$$

$$\textbf{DCO}_\textbf{2}: \quad R-COOH \rightarrow R^{\cdot} - H + CO_2 \tag{3}$$

The n-alkanes obtained via HDO retain the same number of carbon atoms of starting FFAs and have H_2O as a by-product (see Eq. 1); in contrast, DCO and DCO_2 (see Eq. 2 and Eq. 3) remove one carbon atom from the reacting FFAs as CO or CO_2, respectively [40]. If acid tails in TGs are long enough (e.g., 16 to 24 carbon atoms), resulting n-alkanes are compatible with combustion in diesel ICE. Lighter n-alkanes or isoalkanes can be formed as byproducts from side reactions of long-chain hydrocarbons (cracking or isomerization of n-alkanes) [41,42].

Breaking the C—O bond in the DO process requires catalysts [43]. Typical temperatures and pressures of catalytic DO are in the ranges of 250–450 °C and 1–300 bar [44]. Edible and non-edible vegetable oils are excellent feedstocks for green diesel production, as they possess TGs with long-chain fatty acid residuals, counting 16 to 24 carbon atoms [45]. Using vegetable oils mainly derived from saturated fatty acids reduces H_2 consumption; in that case, the process occurs under milder conditions, limiting undesirable side reactions [13]. Using non-edible oils would overcome ethical issues and competition with food chains [13,15].

Catalysts used in the DO are based on noble or non-noble metals, as usually sorted in literature [13,46]. Noble metals such as Pd, Pt, Rh, Ru are very promising DO catalysts, but their expensiveness hinders their use; in those cases, mono-, bi-, and trimetallic catalysts based on non-noble metals (e.g., Ni, Zn, Co, Mo) are preferred [13,15,46]. Catalysts in both supported and massive forms are proposed for DO, usually synthesized by impregnation and co-precipitation methods, respectively [13,15,46]. As to supports, common choices include alumina, silica, titania, zeolites, aluminosilicates, less usually hydrotalcite, and activated carbon, respectively [13,15,46]. Supported Ni-based, NiMo-based, or noble metal-based catalysts are usual choices in literature. For a more structured comparison among the different types and performances of DO catalysts, please refer to [13,15,46].

Catalysts derived from synthetic Layered Double Hydroxides (LDH) may be suitable for DO, even though few studies [47–49] report their use for green diesel production. In the search for new types of catalysts for DO, repurposing catalysts created for other reactive paths is a very interesting strategy. Velasquez et al. [50] obtained by coprecipitation two trimetallic unsupported catalysts with layered precursor structure of the ϕ_y-type phases (NH_4^+ as the compensation ion) for propane oxidative-dehydrogenation (ODH): ϕ_y Nickel-Cobalt-Molybdenum (henceforth "NiCoMo") and ϕ_y Zinc-Cobalt-Molybdenum (henceforth "ZnCoMo"). From a strictly chemical point of view, ODH and DO have opposite effects since the former is an oxidation and the latter a reduction [13,50]. From the process point of view, there are relevant differences, as ODH is a gas-solid heterogeneous reaction [13,15], and DO is a gas-liquid-solid one [50]. From the development point of view, ODH is still far from commercial implementation (mainly because of the large amount of carbon oxides produced at the temperatures needed to activate the alkanes [50–52]); in contrast, DO spans from laboratory-scale to industrial-scale depending on the used biomass [13]. From the catalyst point of view, ODH requires oxides that work by lattice oxygen/vacancy transfer (Mars Van Krevelen) [50,53], whereas DO relies on reduced phases usually affine with H_2 [13,15]. All these issues make the repurposing of layered Velasquez et al. [50]'s NiCoMo and ZnCoMo from ODH to DO quite challenging, as this operation involves a significant change of employment (from oxidation in a gas-solid packed-bed reactor to reduction in a gas-liquid-solid slurry reactor) and paves the way for usages that already have concrete industrial perspectives.

This work aims to repurpose Velasquez et al. [50]'s NiCoMo and ZnCoMo catalysts, replicating their synthesis and unprecedently testing them for green diesel production through the DO process. Commercial rapeseed oil was selected as the feedstock for DO experiments performed in a stirred batch reactor. Temperature (T), catalyst-to-oil ratio (γ), and reaction duration (t) were the factors investigated for each catalyst, according to an exploratory unreplicated 2^3 factorial design of experiments (DoE) with a replicated center point. Recycling tests were carried out to evaluate the reusability of the catalysts.

2. Materials and methods

Several methods are briefly listed in this section. When further technical information is available in Supporting Materials (SM), an indication is given after the short description of the technique.

2.1. Materials

Commercial rapeseed oil was used as the feedstock in the catalytic DO tests. The oil composition was purposely determined in this work by transesterification, according to AOAC International guidelines [54]. The resulting mixture of Fatty Acid Methyl Esters (FAMEs) was analyzed by a Thermo Trace GC Ultra 7820 Gas-Chromatograph coupled with a Flame Ionization Detector (GC-FID), as detailed in Section A.1 of SM.

The NiCoMo and ZnCoMo catalysts were synthesized by replicating the coprecipitation method proposed by Velasquez et al. [50], also described in Section A.2 of SM.

2.2. Catalysts characterizations

Fourier-Transform InfraRed spectroscopy (FT-IR) was performed on synthesized catalysts by PerkinElmer Spectrum Instrument in Attenuated Total Reflection (ATR) mode, covering the range from 4000 to 400 cm^{-1}. Velasquez et al. [50] report FT-IR performed on catalysts in transmission mode.

Inductively Coupled Plasma-Mass Spectrometry (ICP-MS) was performed to assess the content of metals in the NiCoMo and ZnCoMo catalysts, in both as-synthesized and after-test states. iCAP TQ (ThermoScientific) with a triple quadrupole MS detector was used. Further details are in Section A.3 of SM.

X-Ray Diffraction (XRD) was carried out on as-synthesized catalysts to detect crystalline phases, using a Bruker AXS D8 ADVANCED X-ray diffractometer, employing CuKα1 radiation in a Bragg-Brentano geometry. The recorded Bragg angle ranged from 20° to 90° with a scanning step of 0.0158° and a sampling time of 1 s per step.

N_2-adsorption and desorption isotherms were recorded by MICROMERITICS ASAP 2420 at the boiling point of N_2 (−196 °C). BET (Brunauer-Emmett-Teller) and BJH (Barrett-Joyner-Halenda) methods were used by ASAP 2420 software (version 2.09) to quantify BET specific surface area (S_{BET}), BJH cumulative specific pore volume (V_{BJH}). Details on sample preparations are in Section A.4 of SM.

Particle size distribution (PSD) of as-synthesized NiCoMo and ZnCoMo was recorded by Malvern Mastersizer 2000. The particle retention index was configured to 2.08, with an absorption index set at 1. Water was used as the dispersant.

Scanning Electron Microscopy with Energy Dispersive X-ray Spectroscopy (SEM-EDS) was used to observe the morphological and topological features of the catalysts in both as-synthesized and after-test states. Observations were performed by a Zeiss Gemini SEM 500 microscope equipped with EDS equipment OXFORD AztecLive with Detector Ultim Max 100. Working parameters are summarized in Section A.5 of SM.

Temperature Programmed Reduction (TPR) was performed on NiCoMo and ZnCoMo by a MICROMERITICS AUTOCHEM II 2920 chemisorption analyzer (50 NmL min^{-1} flow rate of 10 %vol H_2 in Ar, 10 °C min^{-1} up to 1000 °C, 30 min dwell at 1000 °C). Further details are in Section A.6 of SM.

Temperature Programmed Desorption of H_2 (TPD-H_2) were performed by the same equipment of TPR. A preparative TPR was operated on samples before TPD, in such a way as to reproduce some conditions (320 °C, 4 h) of the in-situ pre-reduction of catalysts operated before experimental DO tests (see Section 2.3). Then, pulsed-H_2 adsorption up to solid saturation was operated, followed by the actual TPD-H_2 under Ar (50 NmL min^{-1} of Ar, 15 °C min^{-1} up to 500 °C, and a dwell of 30 min at 500 °C). Full details of experimental procedures are described in Section A.6 of SM.

2.3. DO tests for Green Diesel production

All catalytic DO tests of rapeseed oil ("single-run" and "recycling") were performed in a PARR® mini batch reactor (series 4598, total reactor volume of 100 mL).

2.3.1. Single-run DO test procedure and characterization of liquid product

First, the catalyst was activated by in-situ pre-reduction, spending 4 h at 320 °C in the closed reactor filled with an initial H_2 partial pressure of 60 bar at Room Temperature (RT).

For each DO test, about 2 g of rapeseed oil (m_{oil}) were loaded into the reactor and mixed with n-hexane (constant n-hexane/oil mass ratio 10:1), then filling the reactor with H_2 at an initial pressure of 40 bar at RT. At the end of each test, the catalyst was recovered by filtering and washed with n-hexane; the reaction product was recovered and separated from n-hexane, then the mass of the reaction product was measured ($m_{product}$).

A portion of $m_{product}$ was transesterified by the same procedure used for fresh oil (Section 2.1) [54], to convert unreacted TGs in FAMEs. The transesterified sample was then analyzed by an Agilent 7820 A GC-FID (details in SM, Section A.7) using a method that allows identifying single n-alkanes peaks from C_7 to C_{40} and cumulative FAMEs peaks. Unknown peaks in the Agilent 7820 A GC-FID's chromatogram were associated with the compound classes "unsaturated hydrocarbons" (UHC) and "branched hydrocarbons" (BHC) through further sample analyses by a GC–MS (GC model: Varian star 3400cx, MS model: Varian Saturn 2000, details in SM, Section A.7). Peaks left unknown or without particular interest for this work were collected in the class "Others".

Overall, the product mass composition was estimated semi-quantitatively in terms of relative percentage areas of chromatographic peaks of Agilent 7820 A GC-FID, namely $A\%_p$ (with $p = C_i$ for the n-alkane with i carbon atoms; *FAME* for unconverted oil; *UHC* for unsaturated hydrocarbons; *BHC* for branched hydrocarbons; *Others* for unidentified peaks).

To uniformly evaluate the DO performances in the different tests, the following parameters – usually adopted in literature [55–58] – were calculated based on experimental data: product yield ($Y_{product}$, Eq. 4), conversion of TGs (χ, Eq. 5); diesel yield (Y_{diesel}, Eq. 6); catalyst selectivity ($S_{HDO/DCOx}$, Eq. 7).

$$Y_{product} = \frac{m_{product}}{m_{oil}} 100 \tag{4}$$

$$\chi = \left(1 - \frac{m_{product}\ \frac{A\%_{FAME}}{100}}{m_{oil}}\right) 100 \tag{5}$$

$$Y_{diesel} = \frac{m_{product}}{m_{oil}} \sum_{i=15}^{18} A\%_{C_i} \tag{6}$$

$$S_{HDO/DCOx} = \frac{A\%_{C_{18}} + A\%_{C_{16}}}{A\%_{C_{15}} + A\%_{C_{17}}} \tag{7}$$

As to $S_{HDO/DCOx}$ (Eq. 7), it should be noted that it is calculated only on the basis of $A\%_p$. Since the absolute chromatographic areas were manually integrated and appear in both the numerator and denominator of Eq. 7, this parameter may be affected by higher variability, compared to other ones.

2.3.2. Unreplicated 2^3 factorial DoE with replicated center point

Considering that the testing of NiCoMo and ZnCoMo for DO was unprecedented, the objective of the experiment included a preliminary and exploratory factor screening to identify the main features of DO catalytic action. In light of this, a simple DoE with a low number of levels was a sensible choice [59] for the "single-run" DO campaign; therefore, the lowest possible number of levels per factor was chosen, i.e., 2.

For the sake of DoE simplicity, an effort was directed to select a minimum number of factors able to characterize catalytic action, to minimize the number of "single-run" DO tests. Among several potential design factors [59] (overall pressure, mixing, solvent-to-oil ratio, temperature, catalyst-to-oil ratio, reaction duration, catalyst activation, H_2 available), the authors of this work found that the choice of the number of actual "design factors" [59] – for the exploratory study about NiCoMo and ZnCoMo repurposing to DO – could be restricted to 3: temperature (T); catalyst-to-oil mass ratio (γ); DO duration (t). Mixing (200 rpm), solvent-to-oil mass ratio (10:1), the entire catalyst activation procedure (320 °C, 4 h, under 60 bar at RT of H_2), and the quantity of loaded H_2 for DO (60 bar at RT of H_2) became "held-constant factors" [59]. Overall pressure was left as an "allowed-to-vary factor" [59], given that loaded H_2 quantity was always the same. No "nuisance factors" were sensibly found to justify any blocking (e.g., batches of rapeseed oil and catalysts were the same in the whole campaign). Further details on system features for statistical analysis are in Section 2.3.2.2.

All this considered, an unreplicated 2^3 factorial DoE with 3 replications at the central point was implemented for the "single-runs" DO campaign of each catalyst. This design allowed for the performance of a reduced number of tests per catalyst (11 vs. 16 of a twice replicated 2^3 factorial DoE) while ensuring the possibility of estimating the variability within system responses (Eq. 11). This last feature allowed setting up an ANOVA concerning [59]: (i) the significance of main effects (Eq. 8) and interactions (Eq. 9, Eq. 10) in the first-order regression model with interactions (Eq. 12); (ii) the check about the need of quadratic regression models (Eq. 14). Further details on this subject are in Section 2.3.2.2.

2.3.2.1. Factors, levels, treatments, responses, effects, interactions. The investigated factors and levels were summarized in Table 1: temperature (T) at levels (−) 280 °C and (+) 320 °C; catalyst-to-oil mass ratio (γ) at levels (−) 4 $\%_{w/w}$ and (+) 10 $\%_{w/w}$; DO duration (t) at levels (−) 2 h and (+) 6 h (measured by the moment the reactor reached the desired temperature). The conditions at the central point were: (0) 300 °C, (0) 7 $\%_{w/w}$ catalyst-to-oil ratio, (0) 4 h. Two additional reference tests were performed out of the DoE: (i) a *"blank"* test, without any catalyst at 320 °C for 6 h; (i) a test without catalyst pre-reduction (*"no pre-red"*) at 320 °C, 10 $\%_{w/w}$ catalyst-to-oil, 2 h. The order of factorial tests was randomized for each catalyst.

The upper and lower levels in Table 1 were largely inspired by previous DO process knowledge, e.g., summarized in the review of Lucantonio et al. [13] and Di Vito Nolfi et al. [15]. The resulting ranges were kept relatively large, due to the exploratory nature of the study [59], preferably opting for mild operating conditions which could confer an additional advantage for industrial exploitation . The value of 280 °C can be considered a general low temperature for DO [13,15], whereas 320 °C was a value that may limit the range of milder DO temperatures (of greater potential interest for industrial scale-up, since they are industrially cheaper, safer, less energy intensive). The value of 4 $\%_{w/w}$ can be considered a feasible catalyst-to-oil ratio for DO [13], whereas 10 $\%_{w/w}$ was a conservative choice due to the complete initial unknowledge of catalysts activity for DO. 2 h and 6 h can be considered plausible lower and upper duration limits for a batch DO [13].

Treatments – i.e., experimental runs with a given combination of factors' levels – were coded with the usual nomenclature of 2^k factorial design, according to factors and levels defined in Table 1, e.g.: "*(1)*" is the treatment with all factors A, B, C at their lower level; "*abc*" is the treatment with all factors A, B, C at their higher level; "*a*" is the treatment with A at its higher level, and B and C at their lower; "*ab*" is the treatment with A and B at their higher level and C at its lower; and so on.

The systems responses considered in this work were product composition and DO performance parameters ($Y_{product}$ (Eq. 4), χ (Eq. 5), Y_{diesel} (Eq. 6), and $S_{HDO/DCOx}$ (Eq. 7)). Let us consider the generic response y of the system in the unreplicated 2^3 factorial plan, and name its value due to a given treatment as y *("treatment code")*. For that plan, one can calculate: the main effect of a factor l on y ($2\beta_l$) as in Eq. 8; the effects on y from the interaction of two factors l and q ($2\beta_{lq}$) as in Eq. 9; and the interaction effects on y due to the three interacting factors A, B, C ($2\beta_{ABC}$), as in Eq. 10 [59]. The main effect of factor l ($2\beta_l$) is the difference between the average of responses y when l is high and that when l is low [59]; the interaction effect between factors l and q ($2\beta_{lq}$) is quantified as the half of the difference between the effect of l in the subset of responses y with q at high level and the effect of l in the other subset of responses y with q at low level [59]; ternary interaction

Table 1
Factor and levels investigated in the unreplicated 2^3 factorial DoE with three replications at the center point.

Factor	Quantity	Low level (−)	High level (+)	Medium level (0)
A	T (°C)	280	320	300
B	γ ($\%_{w/w}$)	4	10	7
C	t (h)	2	6	4

between A, B, C ($2\beta_{ABC}$) is the average difference between the AB interaction at the two different levels of C [59].

$$2\beta_l = \begin{cases} \dfrac{y(abc)+y(ab)+y(ac)+y(a)}{4} - \dfrac{y(bc)+y(b)+y(c)+y(1)}{4} \\ \text{with}: l = A \\ \dfrac{y(abc)+y(ab)+y(bc)+y(b)}{4} - \dfrac{y(ac)+y(a)+y(c)+y(1)}{4} \\ \text{with}: l = B \\ \dfrac{y(abc)+y(ac)+y(bc)+y(c)}{4} - \dfrac{y(ab)+y(a)+y(b)+y(1)}{4} \\ \text{with}: l = C \end{cases} \tag{8}$$

$$2\beta_{lq} = \begin{cases} \dfrac{y(abc)-y(bc)+y(ab)-y(b)}{4} - \dfrac{y(ac)-y(c)+y(a)-y(1)}{4} \\ \text{with}: l = A, q = B \\ \dfrac{y(abc)-y(bc)+y(ac)-y(c)}{4} - \dfrac{y(ab)-y(b)+y(a)-y(1)}{4} \\ \text{with}: l = A, q = C \\ \dfrac{y(abc)-y(ac)+y(bc)-y(c)}{4} - \dfrac{y(ab)-y(a)+y(b)-y(1)}{4} \\ \text{with}: l = B, q = C \end{cases} \tag{9}$$

$$\beta_{ABC} = \frac{y(abc)-y(bc)-(y(ab)-y(b))}{4} - \frac{y(ac)-y(c)-(y(a)-y(1))}{4} \tag{10}$$

2.3.2.2. ANOVA and regression of empirical models. According to Montgomery [59], for unreplicated 2^k factorial DoE with n_C observations at the center point, the pure error mean square (MS_E) of a given response y can be estimated by its central observations y_{jC} with $n_C - 1$ degrees of freedom ($j = 1, \ldots, n_C$, with $\bar{y}_C$ as the arithmetic mean of y_{jC}), as in Eq. 11. The quantity MS_E (Eq. 11) is the experimental variability, reference for each F-test in the ANOVA that determines the statistical significance of effects and interactions, as defined in Section 2.3.2.1.

$$MS_E = \frac{\sum_{j=1}^{n_C}\left(y_{jC}-\bar{y}_C\right)^2}{n_C-1} \tag{11}$$

Due to the explorative nature of the current work, a relatively large significance level up to $\alpha = 10$ % was considered acceptable in ANOVA, in order to avoid hasty exclusions of effects from the set of significative ones [59].

Thanks to the use of a 2^k factorial DoE, one can represent each response y of the investigated system by a regressed "first-order main-effects model with interactions" (Eq. 12, with β_0 = grand average of y observations; β_l = half of main effect of factor l (Eq. 8); β_{lq} = half of interaction effect between factors l and q (Eq. 9); β_{ABC} = half of interaction effect between A, B, C (Eq. 10); x_l = coded design variable of factor l: $-1 \le x_l \le +1$, i.e., normalized within the range of levels for factor l; ε = experimental error) [59]. For each response y, only β's corresponding to statistically significant effects according to ANOVA were included in the empirical regression model in Eq. 12.

$$y = \beta_0 + \sum_{l=1}^{k}\beta_l x_l + \sum\sum_{l<q}\beta_{lq}x_l x_q + \beta_{lq}x_A x_B x_C + \varepsilon \quad \text{with}: l, q = \text{A, B, C} \tag{12}$$

An additional peculiar advantage comes with unreplicated 2^3 factorial DoE with replications at central point [59]: a single-degree-of-freedom sum of squares is given by Eq. 13, to investigate the need to consider pure quadratic curvature ($SS_{pure\ quadratic}$) in the empirical regression model. In Eq. 13 $n_F = 2^k$ is the number of unreplicated factorial observations of the response y, and $\bar{y}_F$ is the arithmetic mean of factorial observations.

$$SS_{pure\ quadratic} = \frac{n_F n_C\left(\bar{y}_F - \bar{y}_C\right)}{n_F + n_C} \tag{13}$$

The ratio $SS_{pure\ quadratic}/MS_E$ is a statistic for an additional F-test incorporated into the ANOVA of the unreplicated factorial observations of response y, with the hypotheses in Eq. 14: when the F-test on pure quadratic fails to reject the null hypothesis H_0 (Eq. 14), the response y can be modeled with "first-order main effects model with interactions" (Eq. 12); otherwise (H_0 rejected, so H_1 true, Eq. 14), y should be better modeled with a "second-order model" (Eq. 15, with β_{ll} = pure quadratic coefficient of factor l), which requires DoE more complex than the one adopted here for the regression of its β coefficients, such as Central Composite Designs (CCD) [59].

$$H_0 : \sum_{l=1}^{k}\beta_{ll} = 0; H_1 : \sum_{l=1}^{k}\beta_{ll} \neq 0 \tag{14}$$

$$y = \beta_0 + \sum_{l=1}^{k}\beta_l x_l + \sum\sum_{l<q}\beta_{lq}x_l x_q + \sum_{l=1}^{k}\beta_{ll}x_l^2 + \varepsilon \tag{15}$$

ANOVA and the abovementioned hypothesis testing were applied to all measured/calculated responses: $Y_{product}$, χ, Y_{diesel}, $S_{HDO/DCOx}$, and product composition.

2.3.3. Recycling tests

Four sequential DO runs were performed on NiCoMo and ZnCoMo (from now on called *Test_Rr*, with $r = 1, 2, 3, 4$), to evaluate the reusability of catalysts. Those recycling tests occurred under the set of experimental conditions {T, γ, t} that gave the best results with the shortest duration during the "single-run" DO campaign. For both NiCoMo and ZnCoMo catalysts, {T, γ, t} corresponded to conditions of treatment "*ab*" (320 °C, 10 $\%_{w/w}$ catalyst-to-oil, 2 h).

For each catalyst, the first DO run (*Test_R1*) occurred exactly as already described in Section 2.3.1. At the end of *Test_R1*, the used catalyst was recovered by filtering, washed with n-hexane, and dried under vacuum at 50 °C overnight. Due to catalyst losses during recovery operations, the amounts of oil and n-hexane in the subsequent *Test_R2* were adjusted to keep the same γ and n-hexane/oil mass ratios. No pre-reductions were performed before *Test_R2*; except for this and the modification of absolute quantities of reactants and reactives, *Test_R2* occurred with the same procedure described in Section 2.3.1. All methods used between the end of *Test_R1* and that of *Test_R2* were applied to run *Test_R3* and *Test_R4*.

The liquid product of each *Test_Rr* was characterized as described in Section 2.3.1. The values of $Y_{product}$ (Eq. 4), χ (Eq. 5), Y_{diesel} (Eq. 6), $S_{HDO/DCOx}$ (Eq. 7) and products composition after each cycle were quantified and compared to observe the stability of the catalysts for DO. Catalyst characterizations (ICP-MS to investigate active phases loss, SEM-EDS to check morphological-topographic changes, XRD to check crystalline structural modifications) were carried out after *Test_R4*.

Table 2
Composition of commercial rapeseed oil in terms of Area % of chromatographic peaks. Cx:y is a fatty acid with x carbon atoms and y double bonds.

Fatty Acid	Species	Area %
Palmitic acid	C16:0	4.9
Stearic acid	C18:0	1.7
Oleic acid	C18:1	64.5
Linoleic acid	C18:2	19.5
Linolenic acid	C18:3	7.3
Arachidonic acid	C20:0	0.6
Cis-9-Eicosenoic acid	C20:1	1.2
Erucic acid	C22:1	0.3

3. Results and discussion

3.1. Feedstock composition

Table 2 shows the composition of the investigated fresh rapeseed oil, expressed as fatty acids percentages. The fresh rapeseed oil was mainly composed of fatty acids with 16 and 18 carbon atoms, with traces ranging from 20 to 22. Therefore, one can figure out that phenomena described from Eq. 1 to Eq. 3 mainly regard R-COOH with 16 and, most of all, 18 carbon atoms in the case of tests discussed in this work; this explains the choice of carbon numbers in the definitions of $S_{HDO/DCOx}$ (Eq. 7) and Y_{diesel} (Eq. 6).

3.2. Characterizations of as-synthesized catalysts

3.2.1. Validation of catalysts synthesis

Several results of characterizations performed in this work on NiCoMo and ZnCoMo can be compared to those of Velasquez et al. [50] to verify the success of replicating their coprecipitation method. Those original characterization results of this work which concerned techniques already used by Velasquez et al. [50] were collected in Supplementary Materials (SM); only comments on the related comparisons were reported in the following.

FT-IR ATR spectra of current NiCoMo and ZnCoMo (Fig. S.1 of SM) qualitatively aligned with those in "FigureS1(b)" by Velasquez et al. [50]: similar bands were found within 950–750 cm^{-1} (symmetric and asymmetric O-Mo-O stretching [50]) and 700–400 cm^{-1} (stretching vibrations of Co/Ni/Zn-O-Mo [50]); differently from Velasquez et al. [50], in the current samples there were not peaks within 4000–1000 cm^{-1} (zones of organic components' peaks), since they were examined in calcined state.

The XRD patterns of current NiCoMo and ZnCoMo (Fig. S.2 of SM) highlighted identical structures with a high crystallinity for both samples, with no peaks beyond 65°. Complete crystal similarity emerged with diffractograms in "Fig. 2b" by Velasquez et al. [50] in the common range 20–40°, attributed to the phase β-$CoMoO_4$ [50]

Table 4
S_{BET}, V_{BJH}, and d_{BJH} of NiCoMo and ZnCoMo.

Sample	S_{BET} (m^2/g)	V_{BJH} (cm^3/g)	d_{BJH} (nm)
NiCoMo	45	0.09	6
ZnCoMo	39	0.11	5

Table 3 shows the ICP-MS results of as-synthesized NiCoMo and ZnCoMo: molar ratios of metals differ acceptably from expected nominal values, with a relative slight excess of Co on Mo. It is worth noting that Ni or Zn experimentally are a minoritarian part of the respective obtained solids (about 1 atom of Ni or Zn for each 10 of Co and 10 of Mo, Table 3).

As to pores properties (better discussed in Section 3.2.3), it is worth stressing that S_{BET} of current NiCoMo and ZnCoMo (Table 4) were coherent with those reported by Velasquez et al. (32 and 27 m^2/g, respectively) [50].

Concerning TPR profiles (commented in detail in Section 3.2.5), trends of current NiCoMo and ZnCoMo (Fig. S3 of SM) were in agreement with the literature of their original synthesis [50]. The reduction temperatures reported in "Fig. 3b" by Velasquez et al. [50] are higher, probably because of the different particle sizes of their catalyst (not indicated in [50]) or the different TPR analysis conditions (30 mL min^{-1} and 10 °C min^{-1} in [50] vs. of 50 mL min^{-1} and 10 °C min^{-1} in this study).

Overall, the characterization results collected in this subsection allowed considering the replication of NiCoMo and ZnCoMo syntheses as successful and well-controlled.

3.2.2. PSD results

The PSD of NiCoMo (Fig. 1 (a)) was multimodal, with bells between about 0.3–2.5 μm, 3–150 μm, and 150–700 μm. The PSD of ZnCoMo (Fig. 1 (b)) was closer to unimodal features, with one approximate bell extended in the range 0.3–600 μm, and minor shoulders corresponding to the multimodality of Fig. 1 (a). Corresponding notable diameter percentiles are in Table S1 of SM. The Sauter mean diameter *d(3,2)* were 6 μm and 7 μm for NiCoMo and ZnCoMo, respectively: this should mitigate intraparticle mass-transport resistances in DO.

3.2.3. Pores analyses

The N_2-physisorption isotherms of NiCoMo are in Fig. 2 (a): data suggested that this catalyst had a slightly porous nature. The shape of isotherms was associated with the IUPAC type IV(a) isotherm (mesoporous materials) [60] because of the presence of the hysteresis (Fig. 2 (a)), and to IUPAC Type II (macroporous or nonporous adsorbents) [60] because of its terminal asymptotical part at high relative pressures (Fig. 2 (a)). The hysteresis shape in Fig. 2 (a) was associated with IUPAC Type H_2(b) (observed for complex pores structures with mesoporosity) [60].

Table 3
Results of NiCoMo and ZnCoMo analysis by ICP-MS in terms of elemental molar ratios; conditions of treatments (1) and "ab" are in Table 6.

	Ni/Mo (mol/mol)	*Ni/Co (mol/mol)*	*Co/Mo (mol/mol)*
Nominal	0.09	0.11	0.85
As-synthesized	0.08	0.08	1.03
NiCoMo post-treatment "(1)"	0.10	0.11	0.94
NiCoMo post-treatment "ab"	0.10	0.11	0.95
NiCoMo post Test_R4	0.05	0.07	1.37

	Zn/Mo (mol/mol)	*Zn/Co (mol/mol)*	*Co/Mo (mol/mol)*
Nominal	0.09	0.11	0.85
As-synthesized	0.13	0.11	1.26
NiCoMo post-treatment "(1)"	0.12	0.11	1.06
NiCoMo post-treatment "ab"	0.10	0.09	1.10
ZnCoMo post Test_R4	0.11	0.09	1.27

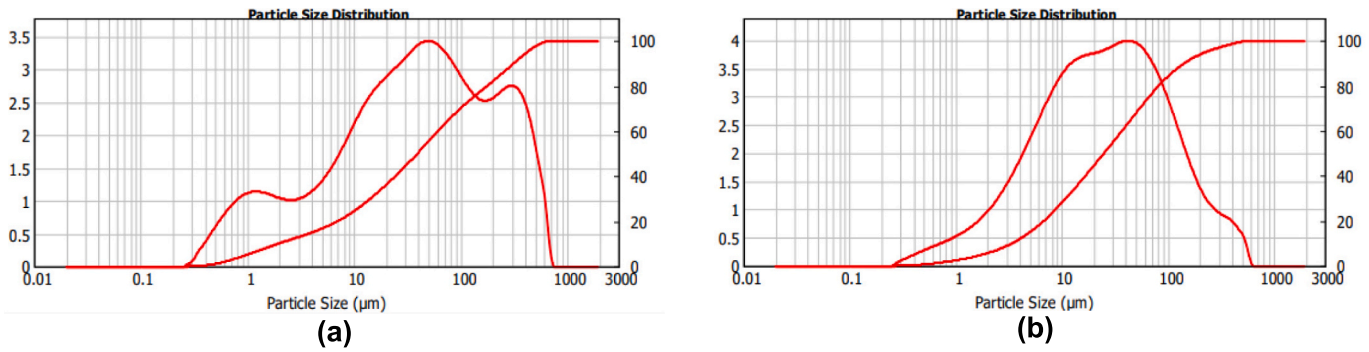

Fig. 1. Particle Size Distribution (PSD) of (a) NiCoMo and (b) ZnCoMo.

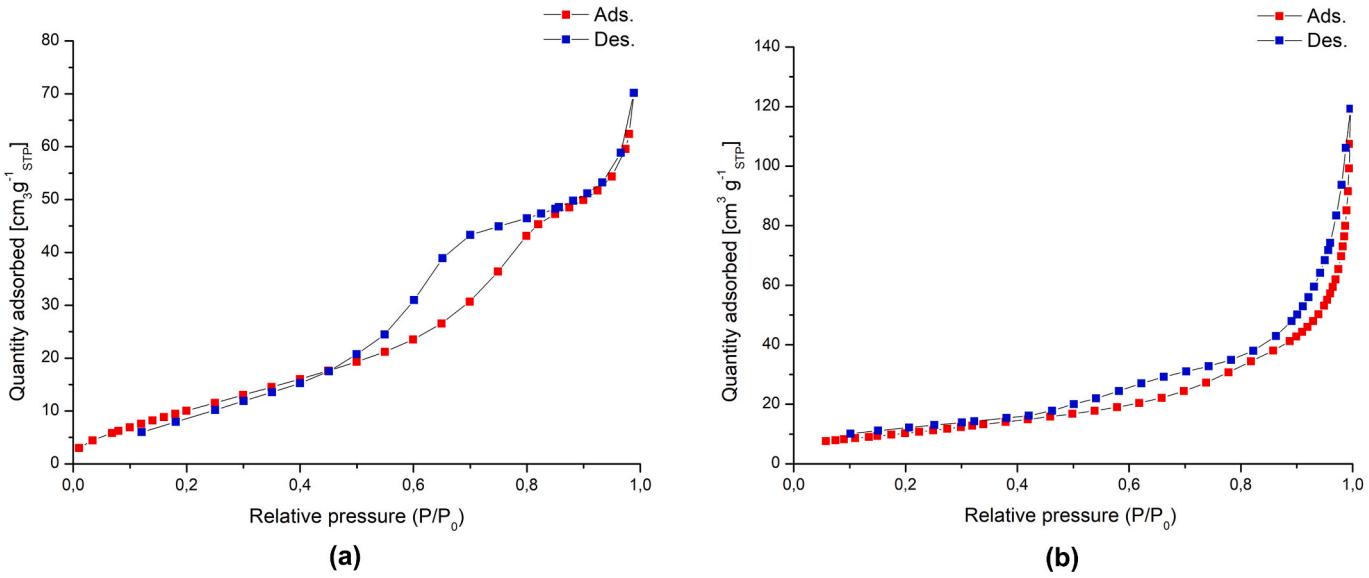

Fig. 2. N_2-physisorption isotherm of as-synthesized (a) NiCoMo and (b) ZnCoMo.

The N_2-physisorption isotherm of the ZnCoMo catalyst (Fig. 2 (b)) presented features of Type IV(a) (hysteresis) and Type II (asymptote at high relative pressures) [60], with the latter having a more significant influence compared to Fig. 2 (a). For ZnCoMo, one could expect a slightly porous material, too.

The S_{BET}, V_{BJH}, and d_{BJH} values of NiCoMo and ZnCoMo (Table 4) corroborated the qualitative shape-analysis of isotherms in Fig. 2, quantifying features representative of slightly porous materials. The textural properties of NiCoMo and ZnCoMo were close.

3.2.4. SEM-EDS

The morphological arrangement of NiCoMo and ZnCoMo observed by SEM included homogeneously distributed lamellar shapes (Fig. 3 (a) and Fig. 3 (b)), which could indicate a layered structure, proving what was suggested by Velasquez et al. [50] in terms of catalyst structure and confirming the reason of interest for their repurposing to DO (as discussed in the Introduction).. The two EDS analyses (Fig. 3 (c) for NiCoMo and Fig. 3 (d) for ZnCoMo) highlighted that the three component metals were uniformly distributed in both catalysts, matching well with the general purposes of a coprecipitation.

3.2.5. TPR

TPR profiles of NiCoMo and ZnCoMo in Fig. S.3 of SM are in agreement with the literature of their original synthesis [50]. The profiles are similar for the two catalysts, sensibly because Co and Mo are preponderant in both materials (see elemental ratios in Table 3). The quantitative aspects of reducibility are also quite close, with NiCoMo showing an overall H_2 consumption for reduction only slightly higher than that of ZnCoMo (23.5 $mmol_{H2}$ g^{-1} vs. 22.8 $mmol_{H2}$ g^{-1}).

Four peak families were observed: (i) 350–400 °C for both samples; (ii) 630 °C for both samples; (iii) 700 °C for ZnCoMo; (iv) 850–900 °C for both samples. The peak family (i) was associated with the reduction of Ni^{2+} in strong interaction with support [44] or the reduction of Co^{3+} into Co^{2+} [45], since ZnO is nonreducible in the studied conditions but would favor Co^{3+} reduction [61], in agreement with measured specific consumptions of H_2 during TPR. The peak family (ii) could be linked to the reduction of the β-$CoMoO_4$ phase leading to an equimolar mixture of $Co_2Mo_3O_8$ and Co_2MoO_4 [62]. In contrast, the peak families (iii) and (iv) could be associated with the reduction of the metals occurring at higher temperatures [62]. Considering the conditions of DO pre-reduction procedure and tests (see Section 2.3), it is reasonable to assume that $Co_2Mo_3O_8$ and Co_2MoO_4 can be eventually formed in the reaction environment.

3.2.6. TPD-H_2

The preparative TPR profiles (320 °C, 4 h) of NiCoMo and ZnCoMo samples before TPD-H_2 are in Fig. 4 (a).

It is worth to remember that this preparative TPR of samples before TPD-H_2 aimed to mimic as far as possible the actual in-situ pre-reduction operated before each experimental DO test (4 h, 320 °C). The temperature of 320 °C for 4 h did not allow the complete reduction of metal oxides in these samples, according to full TPR up to 1000 °C in Fig. S3 of

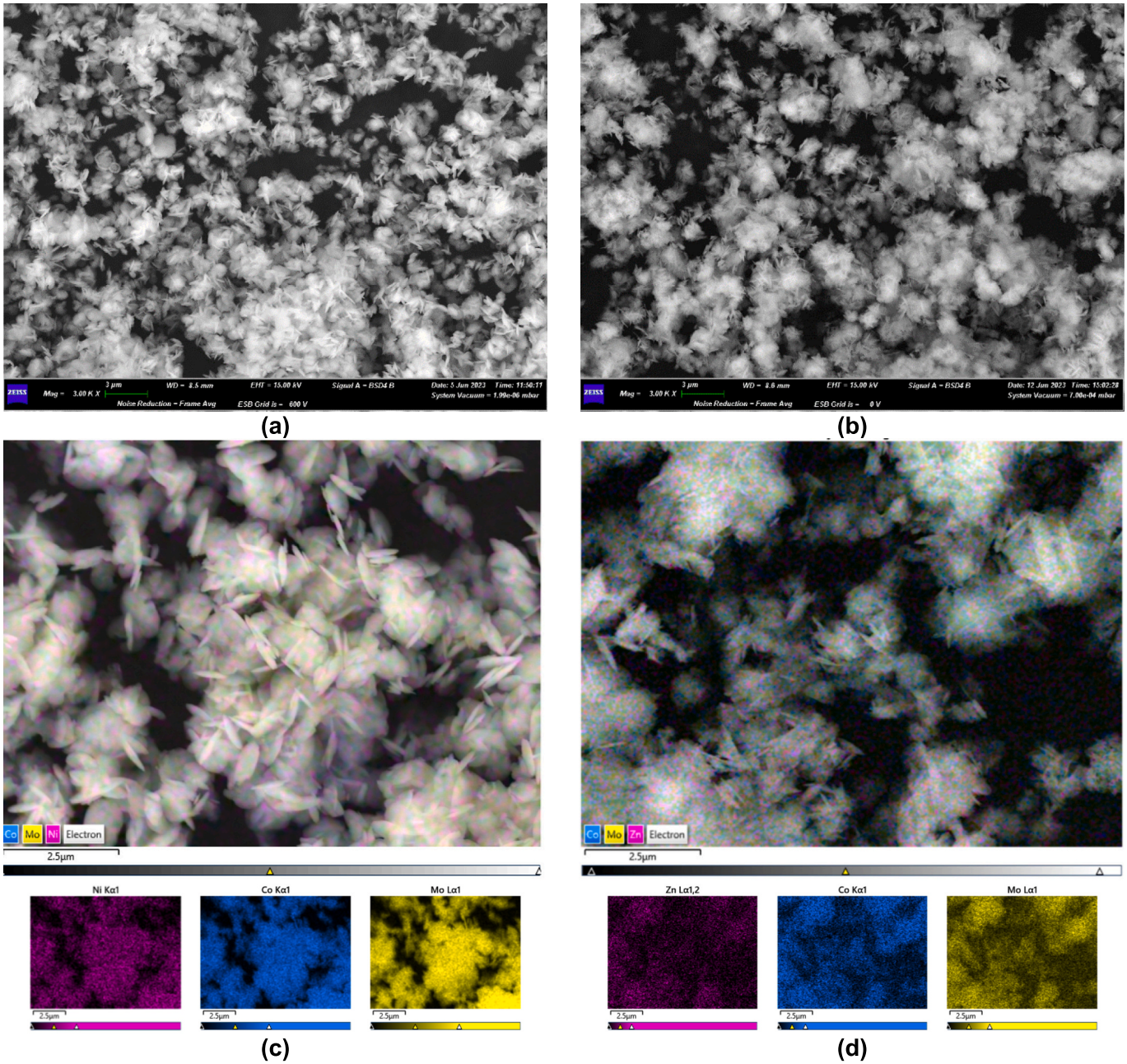

Fig. 3. SEM micrographs at 3000× magnification of: (a) as-synthesized NiCoMo and (b) as-synthesized ZnCoMo. SEM-EDS analyses with elemental maps of: (c) as-synthesized NiCoMo (Ni = magenta; Co = blue; Mo = yellow) and (d) as-synthesized ZnCoMo (Zn = magenta; Co = blue; Mo = yellow). (For interpretation of the references to colour in this figure legend, the reader is referred to the web version of this article.)

SM. However, the conditions seemed sufficient for reducing a part of Ni^{2+} and Co^{3+} previously observed by TPR around 350–400 °C (Fig. S3 in SM); therefore, the first activation of catalysts in experimental tests occurred. In addition, the TPD-H_2 preparative reduction was operated at atmospheric pressure with 10 % vol H_2; in contrast, the actual in-situ pre-reduction operated before each experimental DO run was at an initial H_2 partial pressure of 60 bar at RT. The H_2 consumption for the reduction of NiCoMo in the conditions of Fig. 4 (a) was 1.20 $mmol_{H2}/g$ against 0.073 $mmol_{H2}/g$ for the peak family (i) of TPR in the conditions of Fig. S3 in SM. For ZnCoMo, H_2 consumption for the reduction in these conditions was 2.05 $mmol_{H2}/g$ against 0.50 $mmol_{H2}/g$ for the peak family (i) of TPR in the conditions of Fig. S3 in SM. These values indicated that the preparative reduction step allowed Ni^{2+} and Co^{3+} reduction and the reduction of the mixed CoMo-oxides phase.

The TPD-H_2 profile of NiCoMo and ZnCoMo samples are in Fig. 4 (b, c). The H_2 desorption seemed to be associated with two different active sites because it took place in two steps: a first desorption peak around 175 °C (Fig. 4 (b,c)), and a second one around 475 °C (Fig. 4 (b,c)). This indicated two different chemical bonds of H_2 with the metal surface of each catalyst and then different metal environments. The H_2 desorbed during these steps was quantified in Table 5 for the two catalysts: desorbed H_2 quantities were close for the first (175 °C) and the second TPD-H_2 peak (475 °C) of both catalysts. These strong similarities in desorption temperatures and desorbed H_2 quantities indicated that pre-reduced NiCoMo and ZnCoMo had similar exposed metallic surfaces and metal environments.

The quantities in Table 5 could be in principle utilized to calculate dispersions of H_2-related active sites in NiCoMo and ZnCoMo. The nature of reduced sites may include Ni-, Co-, or Co-Mo-derived ones, as proposed in the discussion of Fig. 4 (a). A precise study on the nature of

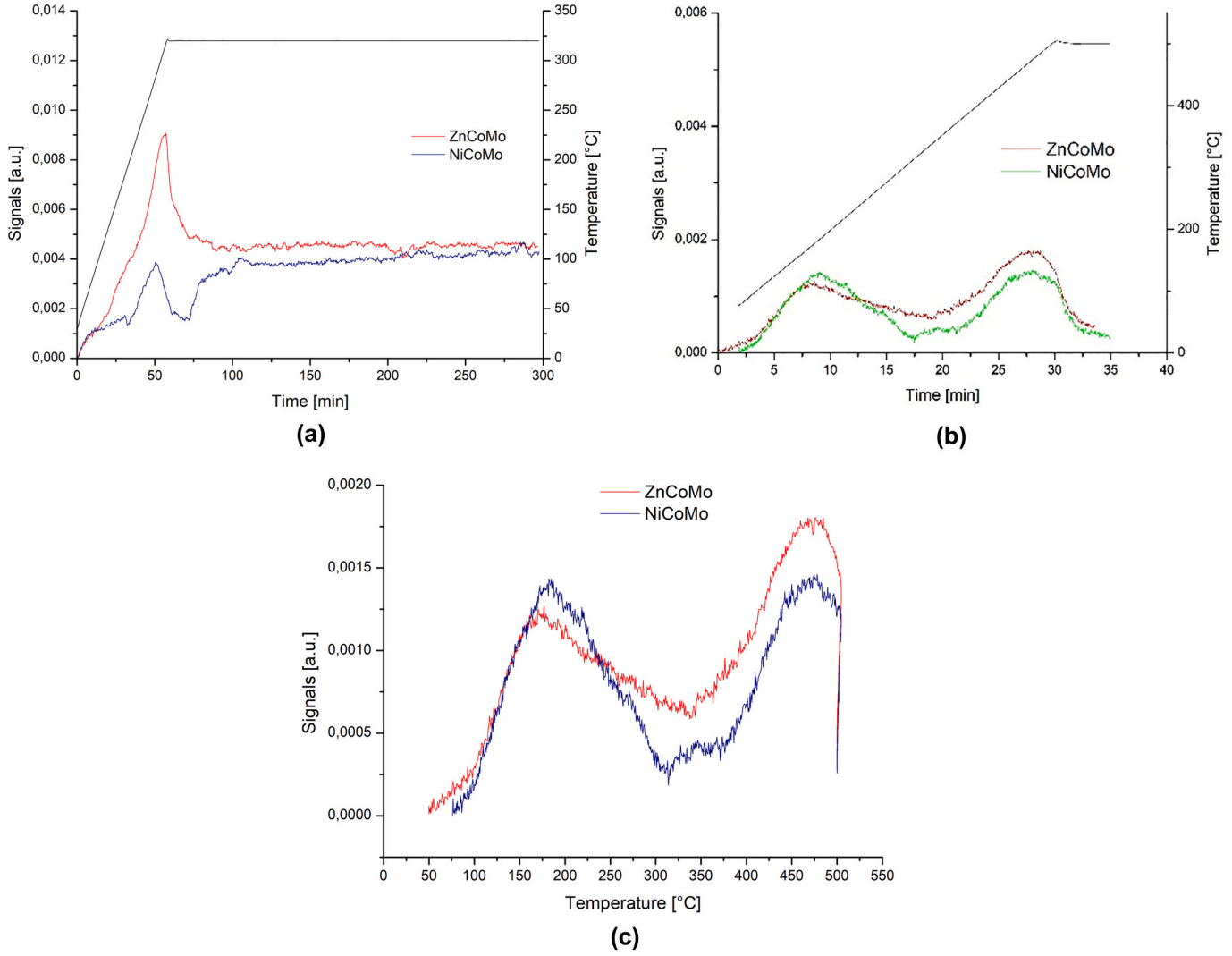

Fig. 4. Results of TPD-H_2: (a) time profiles of TPR preparative procedure (320 °C, 4 h) for NiCoMo and ZnCoMo before TPD-H_2; (b) time profiles of TPD-H_2 for NiCoMo and ZnCoMo; (c) temperatures profiles of TPD-H_2 for NiCoMo and ZnCoMo.

Table 5
H_2 desorption during TPD-H_2 of NiCoMo and ZnCoMo.

Sample	First peak (175 °C) ($mmol_{H2}/g$)	Second peak (475 °C) ($mmol_{H2}/g$)	Total ($mmol_{H2}/g$)
NiCoMo	0.010	0.009	0.019
ZnCoMo	0.008	0.009	0.017

all possible kinds of active sites in the two trimetallic catalysts is not part of the purposes of the current manuscript, which mainly focused on the practical aspects of repurposing NiCoMo and ZnCoMo for DO. In addition, the similarity in results in Table 5 would result in similar calculated overall dispersions, so this parameter would not be particularly influential in the diagnostics of different behaviors.

3.3. Results of DO tests

The experimental campaign of DO was subdivided into two sets: (i) the exploratory factor screening and process characterization by the unreplicated 2^3 factorial DoE with three replications at the center point (according to Table 1); (ii) the recycling tests at conditions with best performances at shorter duration (i.e., 320 °C, 10 $\%_{w/w}$ catalyst-to-oil, 2 h).

In both cases, product composition and DO performance parameters ($Y_{product}$ (Eq. 4), χ (Eq. 5), Y_{diesel} (Eq. 6), and $S_{HDO/DCOx}$ (Eq. 7)) were used to evaluate the experiments. It is worth stressing the primary evaluation criteria:

- Within product compositions, n-alkanes from C_{15} to C_{18} were of main interest for green diesel production, whereas FAMEs indicated unreacted TGs.
- $Y_{product}$ (Eq. 4) quantified the share of initial oil mass that was recovered as a condensed product at the end of each DO run; for instance, $Y_{product}$ lowers because of those TGs carbon atoms lost as propane from the reduction of glyceridic backbone or other light hydrocarbons formed by cracking, allegedly gone in the gas phase.
- χ (Eq. 5) quantified the share of initial oil mass that was converted into something else (not only diesel n-alkanes), i.e., that did not remain in TGs/FFAs forms; therefore, χ could be an indicator of the general activity of the catalysts. Low χ must be accompanied by high values of FAMEs fractions (i.e., unreacted TGs/FFAs), indeed.
- Y_{diesel} (Eq. 6) quantified the share of initial oil mass that became diesel n-alkanes from C_{15} to C_{18}.
- $S_{HDO/DCOx}$ (Eq. 7) was an index of preference among DO reaction paths: the fresh rapeseed oil contained mainly C_{16} and C_{18} fatty acids (Table 2) and no acids with odd carbon atoms, so $S_{HDO/DCOx} > 1$ (Eq. 7) indicated that reactions without loss of carbon (HDO, Eq. 1, forming C_{16} and C_{18} n-alkanes in the current case) were preferred to

Table 6
Experimental results of unreplicated 2^3 factorial DoE with 3 replicated central points (with treatments classified for ANOVA) and of supplementary "blank" and "no-pre-red" tests.

NiCoMo test	A	B	C	treatment	$A\%_{Ci}$ $8 \le i \le 14$	$A\%_{Ci}$ $15 \le i \le 18$	$A\%_{Ci}$ $19 \le i \le 30$	$A\%_{BHC}$	$A\%_{UHC}$	$A\%_{Others}$	$A\%_{FAME}$	$Y_{product}$	χ	Y_{diesel}	$S_{HDO/DCOx}$
	[°C]	[$\%_{w/w}$]	[h]		[%]	[%]	[%]	[%]	[%]	[%]	[%]	[wt%]	[wt%]	[wt%]	[−]
blank	320	0	6		0.00	0.00	0.00	0.00	0.00	14.15	85.85	85.07	26.97	0.00	–
no-pre-red	320	10	2		3.77	37.20	3.56	0.00	3.38	14.07	38.12	86.93	66.87	32.34	2.1
_04	–	–	–	(1)	0.00	37.48	1.94	0.00	1.15	1.15	58.23	89.24	48.03	33.45	1.5
_02	+	–	–	a	3.14	69.87	1.80	6.89	1.69	6.31	10.30	84.09	91.34	58.75	3.0
_06	–	+	–	b	4.94	89.18	3.92	0.35	0.00	0.39	1.22	82.04	99.00	73.16	1.8
_03	+	+	–	ab	4.38	86.77	3.04	4.67	0.28	0.87	0.00	78.39	100.00	68.01	2.4
_08	–	–	+	c	3.74	87.96	3.36	0.37	0.00	0.56	4.00	82.99	96.68	73.00	1.8
_07	+	–	+	ac	3.63	89.05	3.23	2.99	0.24	0.83	0.00	79.95	100.00	71.22	3.9
_05	–	+	+	bc	4.71	91.67	3.29	0.34	0.00	0.00	0.00	77.96	100.00	71.47	1.4
_01	+	+	+	abc	3.02	83.90	2.87	5.62	0.00	4.59	0.00	73.81	100.00	61.92	2.0
_09	0	0	0	central	5.00	88.54	4.43	1.34	0.00	0.71	0.00	81.28	100.00	71.97	2.1
_10	0	0	0	central	4.72	87.05	4.30	3.63	0.00	0.30	0.00	80.05	100.00	69.68	2.9
_11	0	0	0	central	4.01	85.73	3.46	6.39	0.41	0.00	0.00	78.97	100.00	67.70	2.9
ZnCoMo test	**A**	**B**	**C**	**treatment**	$A\%_{Ci}$ $8 \le i \le 14$	$A\%_{Ci}$ $15 \le i \le 18$	$A\%_{Ci}$ $19 \le i \le 30$	$A\%_{BHC}$	$A\%_{UHC}$	$A\%_{Others}$	$A\%_{FAME}$	$Y_{product}$	χ	Y_{diesel}	$S_{HDO/DCOx}$
	[°C]	[$\%_{w/w}$]	[h]		[%]	[%]	[%]	[%]	[%]	[%]	[%]	[wt%]	[wt%]	[wt%]	[−]
blank	320	0	6		0.00	0.00	0.00	0.00	0.00	14.15	85.85	85.07	26.97	0.00	–
no-pre-red	320	10	2		3.74	38.61	9.78	0.00	10.99	0.00	36.88	88.60	67.33	34.20	2.9
_04	–	–	–	(1)	3.39	37.07	3.61	0.00	2.17	8.64	45.13	89.01	59.83	32.99	1.9
_02	+	–	–	a	5.36	85.04	3.88	4.27	1.45	0.00	0.00	76.59	100.00	65.13	2.9
_06	–	+	–	b	6.35	84.76	4.51	1.80	1.51	0.00	1.06	80.16	99.15	67.95	2.3
_03	+	+	–	ab	6.94	83.30	3.74	5.69	0.33	0.00	0.00	76.81	100.00	63.98	2.3
_08	–	–	+	c	1.83	76.94	2.54	0.83	0.00	0.00	17.87	82.77	82.77	63.68	2.2
_07	+	–	+	ac	5.66	89.14	2.99	2.21	0.00	0.00	0.00	76.82	100.00	68.48	2.8
_05	–	+	+	bc	6.00	88.99	3.78	1.23	0.00	0.00	0.00	73.79	100.00	65.66	2.1
_01	+	+	+	abc	7.59	80.88	4.40	5.25	0.00	1.88	0.00	74.35	100.00	60.13	2.6
_09	0	0	0	central	6.24	87.32	3.70	2.52	0.19	0.00	0.00	70.10	100.00	61.24	2.2
_10	0	0	0	central	5.08	89.62	3.63	1.68	0.00	0.00	0.00	78.06	100.00	69.96	2.5
_11	0	0	0	central	4.60	87.19	3.19	2.63	0.00	2.40	0.00	76.80	100.00	66.96	2.7

those with carbon losses (DCO and DCO_2, Eq. 2 and Eq. 3, forming C_{15} and C_{17} n-alkanes in the current case).

3.3.1. *Unreplicated 2^3 factorial DoE with 3 replications at center point*

The results of single-run DO tests according to the DoE described in Section 2.3.2 are summarized in Table 5 for both NiCoMo and ZnCoMo, in terms of product composition and DO performance parameters $Y_{product}$ (Eq. 4), χ (Eq. 5), Y_{diesel} (Eq. 6), and $S_{HDO/DCOx}$ (Eq. 7); the "Test" number labels in Table 6 identify the order of factorial test executions.

3.3.1.1. Qualitative analysis. Several general comments emerged from a qualitative analysis of data in Table 6.

In the "*blank*" test (320 °C, 6 h, no catalyst) there was no conversion of TGs in C_8-C_{14}, C_{19}-C_{30}, and C_{15}-C_{18} n-alkanes, BHC, or UHC (Table 6); therefore, pressurized H_2 and temperature cannot trigger alone the DO processes. This confirmed the need for a proper catalyst to divert chemical species in the DO mechanisms at studied conditions; therefore, everything discussed in the following was attributed to a catalytic action.

The "*no-pre-red*" tests – with NiCoMo or ZnCoMo – produced some transformations ascribable to DO, forming n-alkanes from C_{15} to C_{18} (Table 6). The less satisfying performances of the "*no-pre-red*" test compared to those at homologous conditions (treatments "*ab*", Table 6) confirmed the need for a pre-reduction step for both catalysts (with impacts studied by TPR in Section 3.2.5 and TPD-H_2 in Section 3.2.6). On the other hand, the unreduced NiCoMo and ZnCoMo were partially active ("*no-pre-red*", Table 6), exhibiting some robustness towards the DO process. A more interesting behavior of ZnCoMo was noted, which produced a higher overall fraction of n-alkanes (i.e., fewer by-products) and slightly higher DO performance parameters (Table 6) than NiCoMo.

Values of $Y_{product}$ were always between 70 and 90 % (Table 6), indicating a non-negligible loss of the initial mass of oil as volatile products.

Values of χ were very high (often 100 %) for both catalysts (Table 6), suggesting a general high activity in the domain of experimental conditions investigated. The only exception was treatment (1), with unsatisfyingly low χ values of 48.0 % for NiCoMo and 59.8 % for ZnCoMo, corresponding to higher FAMEs fractions (Table 6). The higher χ of ZnCoMo at prohibitive conditions (treatment (1), Table 6) could be ascribed to a higher intrinsic activity of ZnCoMo. XRD phases, BET specific surfaces, TPR reducibility and TPD-H_2 interactions appeared very similar for the two catalysts; on the other hand, Velasquez et al. [50] found that a higher acidity of ZnCoMo compared to NiCoMo emerged as one of the few actual differences between the two catalysts, measured by TPD-NH_3 [50]; this feature could be related to the higher activity of catalysts in DO. For example, Duan et al. [63] – who studied the effect of Al incorporation into Pd/Al-SBA in DO of sunflower oil – found that an increase in the catalyst acidity enhanced its catalytic DO activity.

Values of Y_{diesel} had ranges of 58.8–73.2 % for NiCoMo and 60.1–70.0 % for ZnCoMo, excluding the treatment (1) that gave about 33 % for both catalysts (Table 6). A general agreement occurred between Y_{diesel} values obtained here and those typical of the literature (60–80 %) [13,15], so the DO performance of NiCoMo and ZnCoMo was evaluated as satisfying in the whole domain of experimental conditions, except for those of treatment (1) (280 °C, 4 $\%_{w/w}$, 2 h). The good performances in terms of Y_{diesel} were caused by high fractions of diesel n-alkanes (C_{15}-C_{18}) in the product (Table 6).

Values of $S_{HDO/DCOx}$ were always higher than 1 for NiCoMo and ZnCoMo (Table 1), i.e., they were both selective towards the HDO pathway in the whole domain of investigated experimental conditions.

This similarity in selectivity matched well with similarities of interactions between H_2 and exposed metallic environments, observed by TPD-H_2 results (Section 3.2.6, Fig. 4(c), Table 5).

As to the product composition (Table 6): (i) the very usual presence of BHC in the products may not be evaluated negatively, since BHC give good cold properties to the green diesel, lowering its freezing point [64]; (ii) the recorded absence (or presence in traces) of UHC was a desirable feature, as UHC lowers the green diesel oxidative stability and promote polymerization [65].

Both catalysts investigated in this work demonstrated remarkable performances for the DO of vegetable oils to green diesel, which were well framed in the context of literature about DO. Ni- and NiMo-based catalysts with different supports [66–68] are presented in the literature to conduct DO at reaction conditions similar to those of this work, using different fatty feedstocks. Lycourghiotis et al. [68] performed several studies on green diesel production over Ni-based catalyst supported by palygorskite, using different oils, at 310 °C, 40 bars of H_2 and 4 h of reaction time: they obtained conversion values between 88 % and 100 %, with diesel n-alkanes content between 10 % and 98 %; at the central treatment point (Table 6), NiCoMo and ZnCoMo ensured total conversion and n-alkanes content close to best obtained by Lycourghiotis et al. [68]. Kordouli et al. [67] tested three NiMo/alumina catalyst, obtained by different methods of synthesis, in the DO process using sunflower oil at 310 °C, 40 bars of H_2 with 9 h of reaction time: they obtained the total conversion of oil into n-alkanes; in particular they obtained 97 % of diesel hydrocarbons in the liquid product; at treatments "*abc*" and "*ac*" (Table 6), NiCoMo and ZnCoMo ensured total conversion and n-alkanes between 80 and 90 %.

Hongloi et al. [66] carried out DO test over Ni-based catalyst with different supports (zirconia, Zeolite Socony Mobil–5, and activated carbon), with palmitic acid as a feedstock, at 270 °C, 10 bars of H_2 for 6 h of reaction time: they obtained 98.3 % of conversion with zirconia as support, 86.2 % with ZSM-5 and 44.7 % with activated carbon as support; DCO and DCO_2 were the main reaction pathways, and the products were mainly composed by C_{15} (around 75 %). At treatments "*c*" and "*bc*" (Table 6), NiCoMo and ZnCoMo ensured conversions between 80 and 100 % and n-alkanes fraction between about 80–90 %.

Experiments [69,70] with Pd/C catalyst under slightly different reaction conditions (300 °C, 10 bars of H_2, and 5–6 h) involved high conversion values (>90 %). The usual employ of supported noble metal catalysts has resulted in conversion values equal to or comparable with those in the present work (Table 6).

3.3.1.2. Statistical analysis. For a quantitative and objective study of recorded experimental data, the influences of investigated factors (A = T, B = γ, C = t, Table 1) were evaluated statistically by calculation of effects and related ANOVA, including an investigation on the significance of pure quadratic terms in empirical response models/response surfaces (Eqs. 14 and 15). Table 7 summarizes the outputs of this statistical study, in terms of: (i) main effects and interactions of A, B, and C factors on product composition and DO performance parameters $Y_{product}$ (Eq. 4), χ (Eq. 5), Y_{diesel} (Eq. 6), $S_{HDO/DCOx}$ (Eq. 7); (ii) estimated significance from ANOVA's F-tests (see Table S.6 of NiCoMo and Table S.7 of ZnCoMo in SM for further information). In the cases of $A\%_{FAME}$ and χ (Eq. 5), F-tests were not performed since no experimental error variance could be estimated by central points. Due to the exploratory nature of this study, weakly significant effects (*P*-value between 0.90 and 0.95, " . " in Table 7) were considered statistically significant (lowering the chances of making a type II error). Statistical comments for each response follow; when not mentioned, an effect was not significant according to Table 7.

Overall, in Table 7 the DO performance parameters $Y_{product}$ (Eq. 4), Y_{diesel} (Eq. 6), $S_{HDO/DCOx}$ (Eq. 7) did not revealed a statistical significance towards the need of quadratic terms to describe them by a surface response. Therefore, in their case the "first-order main-effects model

Table 7
Effects of main factors and interactions from experimental data of unreplicated 2^3 factorial DoE with 3 replicated central points and their significance calculated by F-test in ANOVA (see Table S.6 and Table S.7); Significance P-value intervals: 0 < *** ≤ 0.001 < ** ≤ 0.01 < * ≤ 0.05 <. < 0.1 < no <1.

NiCoMo treatment	$A\%_{Ci}$ $8 \le i \le 14$ [%]		$A\%_{Ci}$ $15 \le i \le 18$ [%]		$A\%_{Ci}$ $19 \le i \le 30$ [%]		$A\%_{BHC}$ [%]		$A\%_{UHC}$ [%]		$A\%_{Others}$ [%]		$A\%_{FAME}$ [%]		$Y_{product}$ [wt%]		χ [wt%]		Y_{diesel} [wt%]		$S_{HDO/DCOx}$ [–]	
A	0.19	no	5.82	*	−0.39	no	4.78	no	0.27	no	2.62	**	−13.29	n.d.	−4.00	*	11.91	n.d.	2.21	no	1.22	.
B	1.63	*	16.78	**	0.69	no	0.18	no	−0.70	.	−0.75	.	−17.83	n.d.	−6.02	*	15.74	n.d.	9.54	*	−0.68	no
AB	−1.32	.	−10.91	**	−0.26	no	0.02	no	−0.13	no	−0.09	no	12.68	n.d.	0.10	no	−11.41	n.d.	−9.55	*	−0.61	no
C	0.66	no	17.32	**	0.51	no	−0.65	no	−0.72	*	−0.68	no	−16.44	n.d.	−4.76	*	14.58	n.d.	11.06	*	0.11	no
AC	−1.09	.	−9.16	*	0.12	no	−0.83	no	−0.14	no	−0.19	no	11.29	n.d.	0.40	no	−10.25	n.d.	−7.87	*	0.13	no
BC	−1.46	.	−17.51	**	−0.91	no	1.12	no	0.58	.	2.35	*	15.83	n.d.	0.44	no	−14.08	n.d.	−14.95	*	−0.51	no
ABC	0.53	no	6.48	*	0.12	no	1.31	no	0.00	no	2.25	*	−10.68	n.d.	−0.65	no	9.75	n.d.	5.67	.	−0.13	no
Pure quadratic		.		*		.		no		no		*		n.d.		no		n.d.		.		no
ZnCoMo treatment	$A\%_{Ci}$ $8 \le i \le 14$ [%]		$A\%_{Ci}$ $15 \le i \le 18$ [%]		$A\%_{Ci}$ $19 \le i \le 30$ [%]		$A\%_{BHC}$ [%]		$A\%_{UHC}$ [%]		$A\%_{Others}$ [%]		$A\%_{FAME}$ [%]		$Y_{product}$ [wt%]		χ [wt%]		Y_{diesel} [wt%]		$S_{HDO/DCOx}$ [–]	
A	2.00	.	12.65	**	0.14	no	3.39	*	−0.48	*	−1.69	no	−16.01	n.d.	−5.33	no	14.60	n.d.	6.85	no	0.55	.
B	2.66	*	12.44	**	0.85	*	1.67	*	−0.44	*	−1.69	no	−15.48	n.d.	−5.03	no	14.10	n.d.	6.85	no	−0.16	no
AB	−0.91	no	−17.43	**	−0.22	no	0.56	no	−0.11	no	2.63	no	15.48	n.d.	3.88	no	−14.10	n.d.	−11.60	.	−0.28	no
C	−0.24	no	11.45	**	−0.51	no	−0.56	no	−1.37	**	−1.69	no	−7.08	n.d.	−3.73	no	6.00	n.d.	7.00	no	0.06	no
AC	0.72	no	−10.60	**	0.39	no	−0.69	no	0.48	*	2.63	no	7.08	n.d.	2.58	no	−6.00	n.d.	−7.25	no	0.00	no
BC	0.39	no	−10.54	**	0.47	no	0.06	no	0.44	*	2.63	no	6.55	n.d.	−0.73	no	−5.50	n.d.	−10.05	.	−0.06	no
ABC	−0.21	no	7.28	*	0.30	no	0.75	no	0.11	no	−1.69	no	−6.55	n.d.	−0.63	no	5.50	n.d.	6.40	no	0.25	no
Pure quadratic		no		**		no		no		*		no		n.d.		no		n.d.		no		no

with interactions" (Eq. 12) generatable by the adopted DoE is suitable for the empirical description of their dependency on the investigated factors.

For NiCoMo, $Y_{product}$ (Eq. 4) was significantly influenced by the main effects of T (A), γ (B), and t (C), all negative (Table 7). The main effects of T (A), γ (B), and t (C) on $Y_{product}$ were negative for ZnCoMo, too, even though neither main effects nor interactions were statistically significant (Table 7). Literature [71] confirms these negative main effects in DO: as the extent of catalytic DO increases (favored by growing T, γ, t), greater quantities of volatile hydrocarbons are formed (e.g., propane from glycerol, light hydrocarbons from cracking) so that $Y_{product}$ decreases; lower temperature and reaction time inhibit the cracking reaction, resulting in higher $Y_{product}$ [71].

The significance of χ (Eq. 5) could not be estimated by replicated central points; anyway, effects on χ were calculated, and notably they had the same signs for both catalysts (Table 7): T (A), γ (B), t (C) all have positive main effects, which sounds plausible; on the other hand, all binary interactions had negative effects. In agreement with the sparsity of effects principle [59], some main effects (and at least some low-order interactions) are more likely to be active.

As to NiCoMo, Y_{diesel} (Eq. 6) was not significantly influenced by T (A), whereas the main effects of γ (B) and t (C) were significant and positive

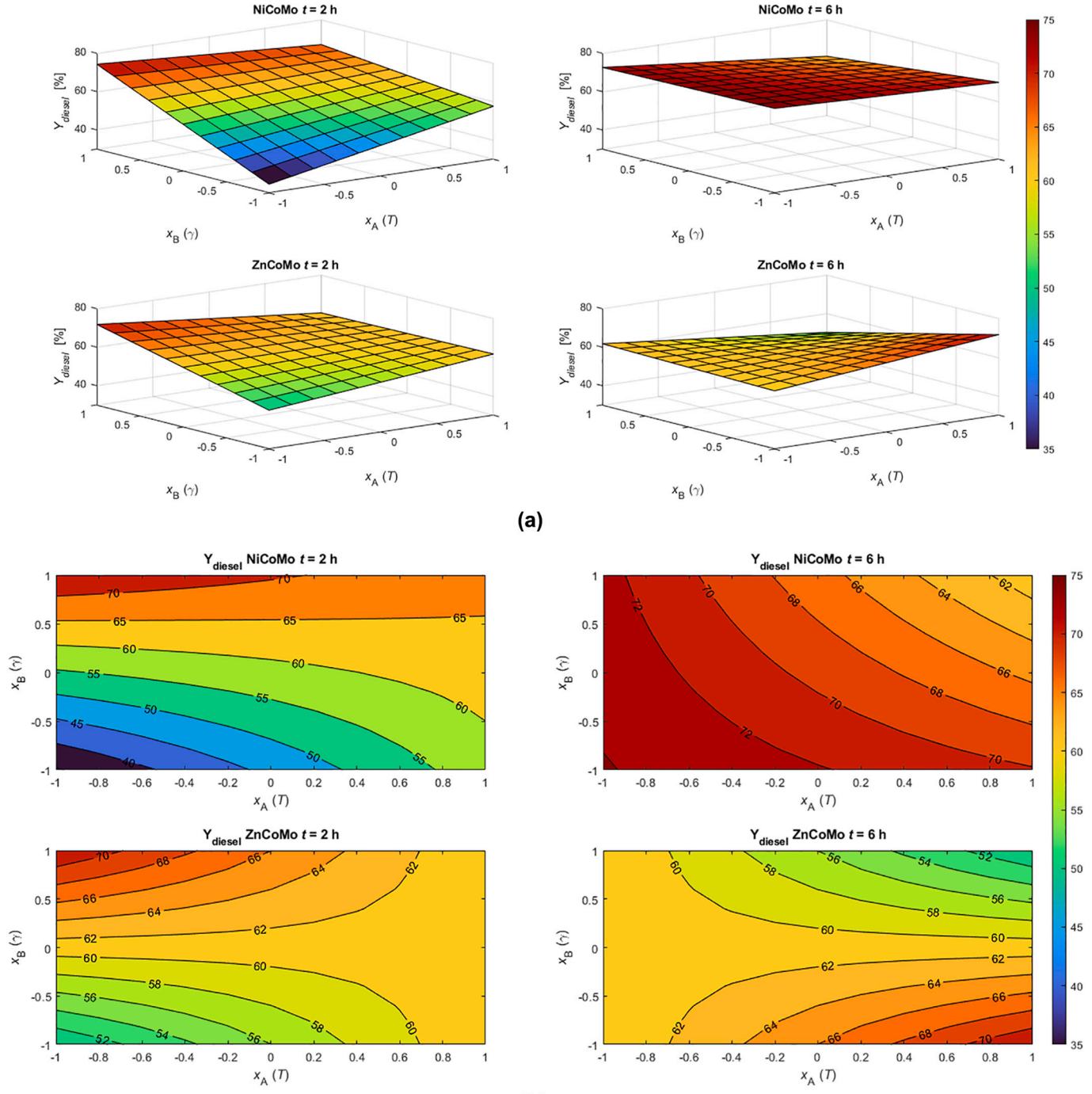

Fig. 5. Regressed response surfaces (a) and related contour plots (b) for Y_{diesel} of NiCoMo (Eq. 16) and ZnCoMo (Eq. 17), as functions of temperature (T), catalyst to oil ratio (γ) and DO duration (t).

(Table 7), i.e., Y_{diesel} grew as γ or t was increased, as found for commercial catalysts in the literature [72,73]; all NiCoMo binary interactions were significant with negative effects on Y_{diesel} (Table 7). Concerning ZnCoMo, only binary interactions of γ with T or t (AB and BC) were weakly significant, with negative effects (Table 7). Overall, the negative effects of binary interactions on Y_{diesel} (Eq. 6) may indicate that the combined increase of investigated factors may favor secondary reactions; this seems in partial agreement with some significant positive effects of binary interactions on the fractions of non-alkane components in the products, e.g., positive significant effects of interaction BC on "others" for NiCoMo, or of AC and BC on "UHC" for ZnCoMo (Table 7). Considering that the Y_{diesel} (Eq. 6) is one of the main parameters in terms of evaluation of DO success, it is worthy to further emphasize the results of the related statistical analysis. Once the non-significant effects and interactions are neglected from the "first-order main-effects model with interactions" (Eq. 12), the specific cases of NiCoMo and ZnCoMo are described by Eq. 16 and Eq. 17 respectively, that originate the surface responses in Fig. 5.

$$Y_{diesel}(NiCoMo) = 63.91 + 4.77\,x_B + 5.53\,x_C - 4.78\,x_A\,x_B - 3.94\,x_A x_C - 7.48\,x_B\,x_C + 2.84\,x_A x_B x_C \quad (16)$$

$$Y_{diesel}(ZnCoMo) = 61.00 - 5.80\,x_A\,x_B - 5.03\,x_B\,x_C \quad (17)$$

Fig. 5 suggested that: (i) if a short DO batch duration is desired (or a higher space velocity in an equivalent continuous process), one has to keep lower temperatures and higher catalyst-to-oil ratios with both catalysts to maximize Y_{diesel}; (ii) if a low catalyst-to-oil ratio is desired, one have to increase the DO duration (or lowering space velocity in equivalent continuous process) with both catalysts, working at lower temperatures with NiCoMo and higher temperatures with ZnCoMo.

$S_{HDO/DCOx}$ (Eq. 7) was influenced only by T (factor A), positively even though with a very weak significance (Table 7). The "first-order main-effects model with interactions" (Eq. 12) of $S_{HDO/DCOx}$, for the specific cases of NiCoMo and ZnCoMo becomes a straight line, described by Eq. 18 and Eq. 19, respectively. Overall, considering the intrinsic variability of $S_{HDO/DCOx}$ quantification from measurements (see Section 2.3.1), and the low significance of temperature dependency, one can state that NiCoMo and ZnCoMo have very similar selectivity performances. In any case, the higher values reachable by Eq. 19 compared to Eq. 18 would be consistent with the higher acidity of ZnCoMo [50]: higher acidity can promote a greater preference for HDO, as found by Duan et al. [63] for Pd/Al-SBA DO catalysts. They [63] observed that the selectivity towards HDO increased as the acidity of the catalyst was increased, suggesting a correlation between acidity and the possible reaction pathways.

$$S_{HDO/DCO_x}(NiCoMo) = 2.23 + 0.61\,x_A \quad (18)$$

$$S_{HDO/DCO_x}(ZnCoMo) = 2.39 + 0.28\,x_A \quad (19)$$

It is worth noting that $A\%_{Ci}$ with $15 \leq i \leq 18$ and other composition categories had ANOVA results with a statistical F-test significance for the need for a quadratic term in the regression of their response surfaces (Table 7). This suggests that if detailed modelling of liquid product composition is desired, a DoE more complex than the one adopted in this work is needed, e.g., a CCD. In any case, some semiquantitative comments on obtained effects, interactions, and their statistical significance can be performed.

The fraction of diesel n-alkanes in the product ($A\%_{Ci}$ with $15 \leq i \leq 18$, Table 7) was very significantly influenced by all main effects and interactions between T (A), γ (B), t (C) for either NiCoMo or ZnCoMo; noticeably, signs of effects resulted the same for both catalysts (Table 7), suggesting that they can work similarly for DO reactions in agreement with similarities deduced by TPD-H_2 profiles (Section 3.2.6, Fig. 4(c), Table 5). The main effects on $A\%_{Ci}$ with $15 \leq i \leq 18$ were all positive (Table 7): the increase of T (A), γ (B), and t (C) all contribute to the rise of diesel fraction in the product. Binary interactions AB, BC, and AC all have negative effects (Table 7); specifically, phenomena like cracking and isomerization might occur at simultaneous high levels of investigated factors [72,74]. This matched well with comments about the influence of the combined increase of investigated factors on Y_{diesel} (Eq. 6). The ternary interaction ABC had a slightly positive effect (Table 7).

3.3.1.3. Final remarks. As stated in Section 2.3.2, the applied DoE aimed to a factor screening and a preliminary process characterization for the repurposing of NiCoMo and ZnCoMo to DO for green diesel production.

For both catalysts, the pure quadratic terms in the hypothetical surface response were significant only for the diesel n-alkanes fraction ($A\%_{Ci}$ with $15 \leq i \leq 18$), the main product of interest for DO, and some secondary product fractions (Table 7). In addition, all main effects and interactions between T (A), γ (B), and t (C) influenced $A\%_{Ci}$ with $15 \leq i \leq 18$ very significantly for either NiCoMo or ZnCoMo. Considering the relevance of diesel fraction $A\%_{Ci}$ with $15 \leq i \leq 18$ for the evaluation of DO performances, the future use of a DoE that allows regressions of second-order models (Eq. 15) should be considered for a better understanding of influences from T (A), γ (B), t (C). A Central Composite Design (CDD) could be a fast solution: the unreplicated 2^3 factorial DoE with central replications utilized in this work can be extended to a CDD, indeed, by the addition of only 6 runs per catalyst. All three factors analyzed here should be kept for future optimization studies. In the case of particular interest, the number of factors can be extended by promoting some "held-constant factors" of this work (mixing, solvent-to-oil mass ratio, catalyst activation procedure, quantity of loaded H_2 for DO) to actual "design factors".

On the other hand, several responses did not show significant influences by main effects (Table 7), with data of catalysts expressing high-quality performances for most of the domain of experimental conditions (Table 6); the constant 100 % χ of central points was a notable example of this trend (Table 6). Even though this effect did not allow a complete preliminary process characterization of NiCoMo and ZnCoMo towards DO, the collected data fully proved the successful repurposing of NiCoMo and ZnCoMo for DO since factors T (A), γ (B), and t (C) were varied in usual ranges for this reaction [13].

All this considered, NiCoMo and ZnCoMo resulted successfully repurposed for DO. A CDD (by extending the current DoE or even starting a new one with different center and level extensions) could be performed in the future for optimization purposes regarding the use of NiCoMo and ZnCoMo to produce green diesel by DO. The search for optimal working points at lowered T (A), γ (B), and t (C) could be an interesting objective: low levels of those parameters could improve the overall sustainability of the related DO process and diminish negative interaction effects.

3.3.2. Results of recycling tests

For both catalysts, the conditions of treatment "ab" (320 °C, 10 $\%_{w/w}$ catalyst-to-oil, 2 h) were selected for the recycling tests; indeed, those conditions gave the best results in terms of product composition, conversion, and diesel yield, at minimized reaction time. Four cycles were performed. Fig. 6 summarizes the results of recycling tests in terms of $Y_{product}$ (Eq. 4), χ (Eq. 5), Y_{diesel} (Eq. 6), $S_{HDO/DCOx}$ (Eq. 7) and product compositions for both catalysts; corresponding numerical data is collected in Table S2 of SM.

NiCoMo and ZnCoMo ensured a 100 % χ for all their four DO cycles (Fig. 6 (a) and Table S2 of SM). This was a significant result, as it demonstrated the stability of the catalysts in promoting the complete conversion of TGs without experiencing significant losses in catalytic activity.

The $Y_{product}$ appeared approximatively constant throughout the four cycles, with a slight growing trend between 75 and 80 % (Fig. 6 (a,b) and Table S2 of SM).

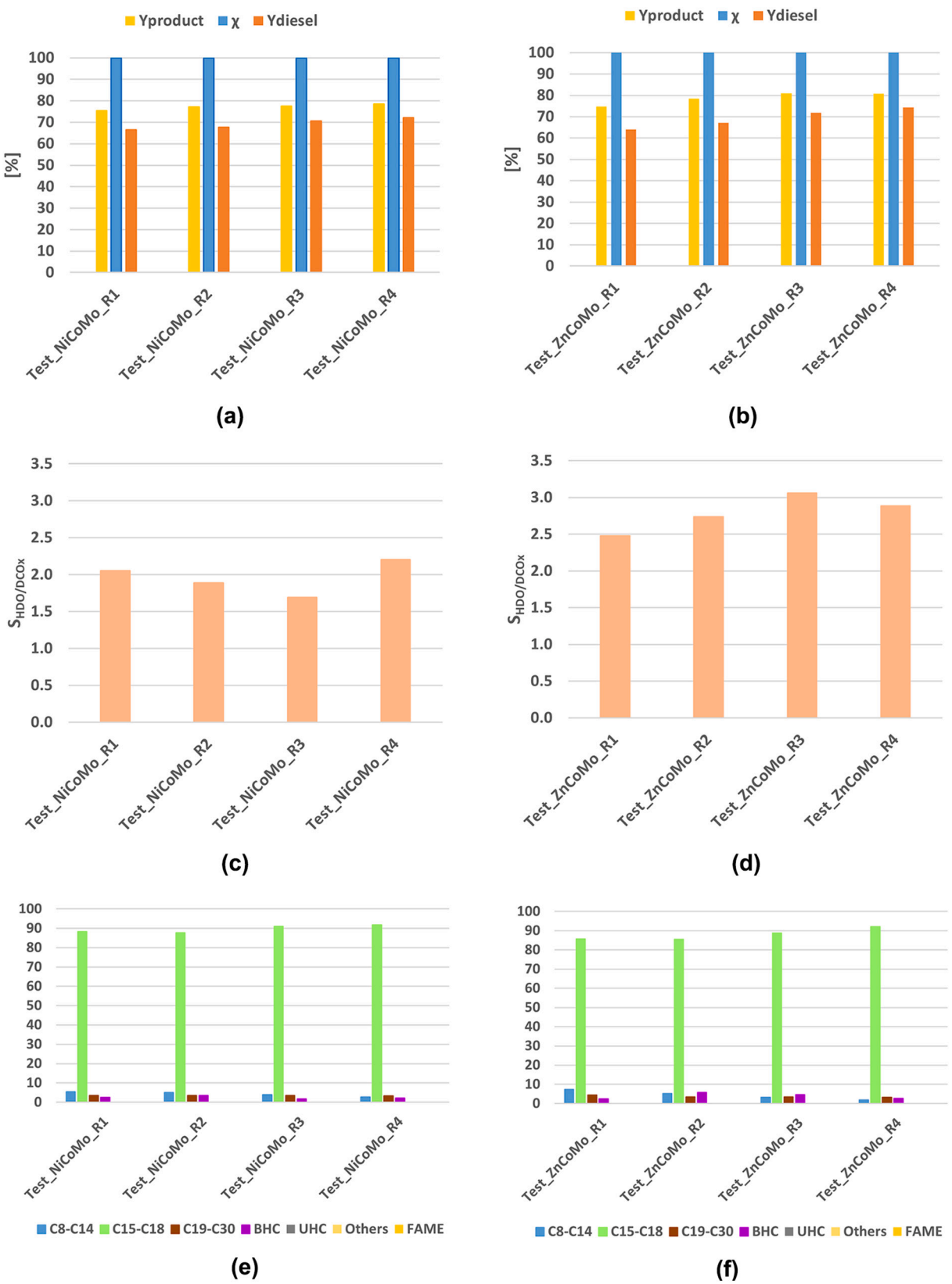

Fig. 6. Results of recycling tests (320 °C, 10 %w/w catalyst-to-oil, 2 h): (a) NiCoMo conversion (χ, Eq. 5), diesel yield (Y_{diesel}, Eq. 6), and product yield ($Y_{product}$, Eq. 4); (b) ZnCoMo conversion (χ, Eq. 5), diesel yield (Y_{diesel}, Eq. 6), and product yield ($Y_{product}$, Eq. 4); (c) NiCoMo selectivity ($S_{HDO/DCOx}$, Eq. 7); (d) ZnCoMo selectivity ($S_{HDO/DCOx}$, Eq. 7); (e) product composition with NiCoMo; (f) product composition with ZnCoMo. Test_(catalyst)_*Rr* is the r^{th} DO cycle with the indicated catalyst.

The Y_{diesel} ensured by both catalysts had a slightly increasing trend, from 66.6 % to 72.2 % for NiCoMo (Fig. 6 (a,b) and Table S2 of SM) and from 64.1 % to 74.4 % for ZnCoMo (Fig. 6 (a,b) and Table S2 of SM).

The ZnCoMo catalyst had a general superior performance in terms of $S_{HDO/DCOx}$ (Fig. 6 (c,d) and Table S.2 of SM), with values always higher than respective ones of NiCoMo, cycle by cycle; in addition, ZnCoMo experienced an increase of $S_{HDO/DCOx}$ (Fig. 6 (b,c) and Table S.2 of SM) up to cycle *R3* and a slight reduction in cycle *R4*, whereas NiCoMo exhibited more stable but lower selectivity. These data suggested a higher efficiency of the ZnCoMo catalyst in promoting HDO reactions, in agreement with considerations about the higher acidity of ZnCoMo proposed in the discussion in Section 3.3.1.2.

Both catalysts exhibited similar patterns in terms of product composition (Fig. 6 (e,f) and Table S2 of SM),: (i) $A\%_{Ci}$ ($8 \leq i \leq 14$) decreased from cycle R1 to cycle R4, with the reduction being more pronounced for ZnCoMo; (ii) $A\%_{Ci}$ ($19 \leq i \leq 30$) and $A\%_{BHC}$ remained relatively stable throughout cycle R1 and the subsequent cycles; (iii) $A\%_{Ci}$ ($15 \leq i \leq 18$), the fraction of the main product of interest for this

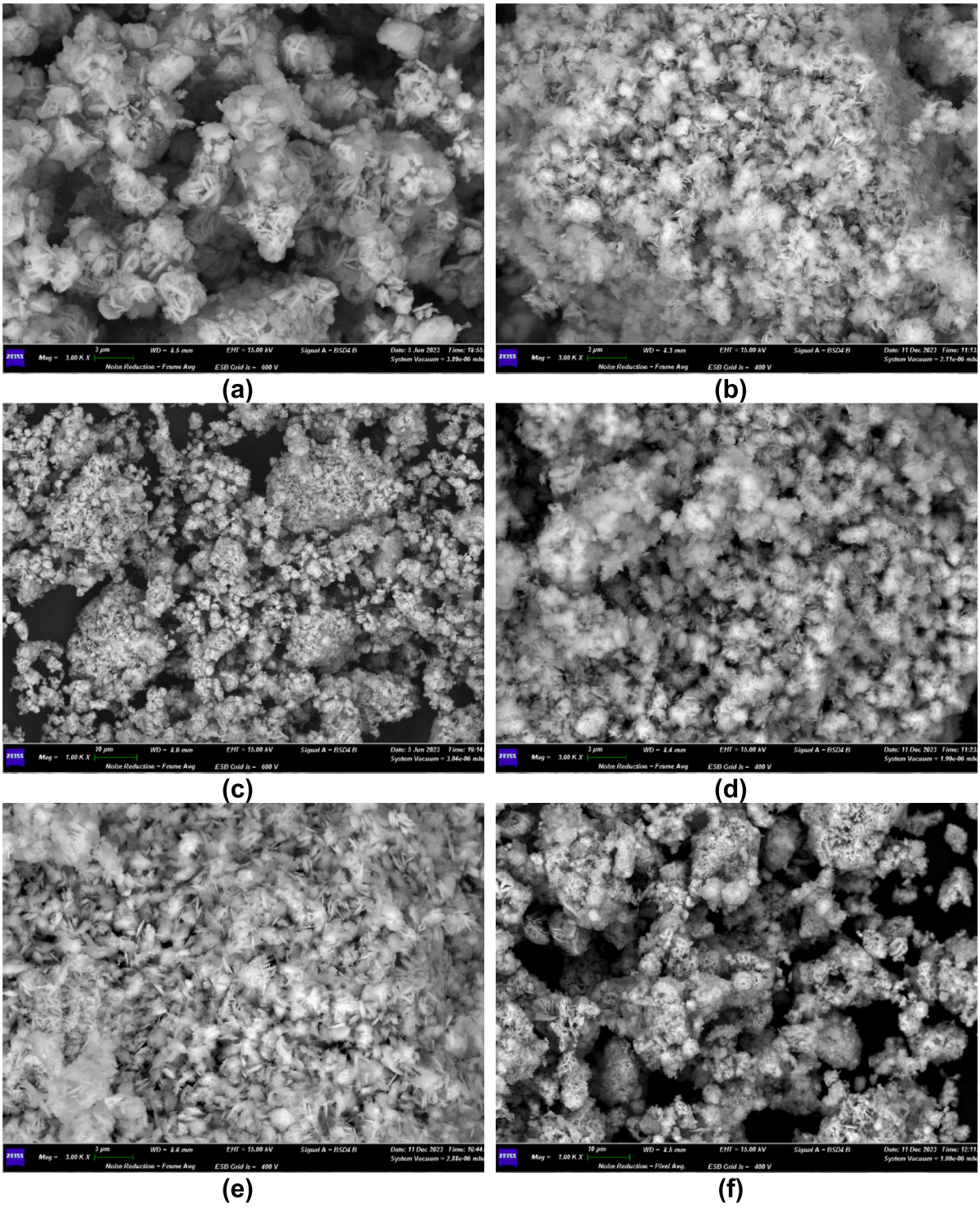

Fig. 7. SEM micrographs of NiCoMo and ZnCoMo after tests: (a) NiCoMo after treatment "ab"; (b) ZnCoMo after treatment "ab"; (c) NiCoMo after treatment (1); (d) ZnCoMo after treatment (1); (e) NiCoMo after Test_R4; (f) ZnCoMo after Test_R4.

work, increased from *R1* to *R4*, with an increment of nearly 4 % for NiCoMo and 8 % for ZnCoMo; (iv) notably, all other possible reaction byproducts were not detected, as indicated by the null values for $A\%_{UHC}$, $A\%_{Others}$, and $A\%_{FAME}$ in Table S2 of SM. The observed decrease in $A\%_{Ci}$ ($8 \leq i \leq 14$) and increase in $A\%_{Ci}$ ($15 \leq i \leq 18$) indicated a shift towards the production of longer-chain n-alkanes in later cycles, noteworthy falling in the window of interest for green diesel production.

Overall, the performances of NiCoMo and ZnCoMo were of remarkable quality and stability throughout the four DO cycles. ZnCoMo had peculiar improvements along with the cyclic usage, as shown by the more pronounced progressive increase of Y_{diesel} and the generally higher values of $S_{HDO/DCOx}$: these two features together result in a better conservation of reactant carbon atoms into desired products (i.e., a better carbon economy).

The good cyclic performances of NiCoMo and ZnCoMo were even more impressive, considering that no pre-reduction was performed before cycles *Test_Rr* with $r = 2$, 3, and 4, i.e., the catalyst robustly behaved during a cyclic utilization without any restoring of initial conditions.

3.4. Catalysts characterization post DO tests

3.4.1. ICP-MS of catalysts post test

The results of ICP-MS on NiCoMo and ZnCoMo after DO tests are in Table 3. In the case of NiCoMo, the comparison between elemental molar ratios in the as-synthesized state and those after one-run tests (treatments "(1)" and "ab", conditions in Table 6) did not show significant changes (Table 3); on the other hand, the results after the overall recycling test (*Test_R4*) indeed suggested a relative loss of Mo (Co/Mo after *Test_R4* higher than in the as-synthesized state, Table 3) and Ni (Ni/Mo and Ni/Co after *Test_R4* lower than in the as-synthesized state, Table 3).

In the case of ZnCoMo, no net trends in elemental ratios were found (Table 3), potentially indicating a higher stability than NiCoMo, especially in cyclic usage.

3.4.2. SEM post-test

Fig. 7 (a,b) show SEM micrographs of NiCoMo and ZnCoMo, respectively, after a one-run test with treatment "ab". This test was selected since it gave satisfying DO performances. The SEM micrographs highlighted that the morphology of the catalysts became flaky, with some residues of the original lamellar distribution (compare Fig. 7 (a,b) with Fig. 3 (a,b)). There were no significant differences in morphology between the two catalysts after treatment "ab".

Fig. 7 (c,d) presents SEM micrographs of NiCoMo and ZnCoMo after treatment (1), corresponding to low DO performances: the micrographs showed that in this case, too, the catalysts became flaky in morphology with some residues of the original lamellar distribution.

Fig. 7 (e,f) shows NiCoMo and ZnCoMo catalysts after the recycling test (*Test_R4*): the morphology of the two catalysts appeared flaky in this case, too; lamellar residues of original as-synthesized catalysts (Fig. 3 (a, b)) were less evident.

Overall, not very marked structural and morphological differences emerged by SEM observations in the different samples after tests that had very different process performances; therefore, the test conditions themselves may be listed among the leading influential causes of the different DO performances with NiCoMo and ZnCoMo.

3.4.3. XRD post test

Fig. 8 compares XRD results of NiCoMo and ZnCoMo at different states: as-synthesized, after single-run tests with treatments "*(1)*" and "*ab*", and after recycling test campaign (i.e., after *Test_R4*).

Fig. 8 showed that the catalysts underwent some variations of crystallites state, which hindered a reliable identification of residual peaks. On the one hand, a hypothesis may be a transition from a more crystalline state in the "as-synthesized" form to a strongly more amorphous one in the post-test samples. On the other hand, the appearance of post-test XRD in Fig. 8 may be associated with very fine crystallite sizes.

Although the catalysts appeared to undergo crystallinity modifications, allegedly during the DO tests, their performances were of high quality concerning both single-run tests (Table 6) and recycling tests (Fig. 6 and Table S.2 of Supporting Material). NiCoMo and ZnCoMo catalyst samples that underwent the treatment "*ab*" once were already modified (Fig. 8), as well as the catalysts samples recycled four times for DO without intermediary prereductions (*Test_R4*, Fig. 8); nonetheless, the catalysts demonstrated stable catalytic activity and remarkable DO performances throughout the whole recycling tests (see Section 3.3.2), despite the crystal modifications that should have occurred since the first cycle (in similitude with samples after treatments "*ab*"). Lin et al. [39] reviewed catalyst design strategies for DO and reported that amorphous alloys (e.g., Ni-Mo-B or Co-Mo-B) often excel in hydrodeoxygenation reactions due to their less ordered structure, which typically has higher potential energy due to metastable states; Lin et al. [39] summarized that the short-range disorder in amorphous metal alloys makes superficially available many unsaturations in coordination atoms, then a higher surface density of active sites is obtained, with

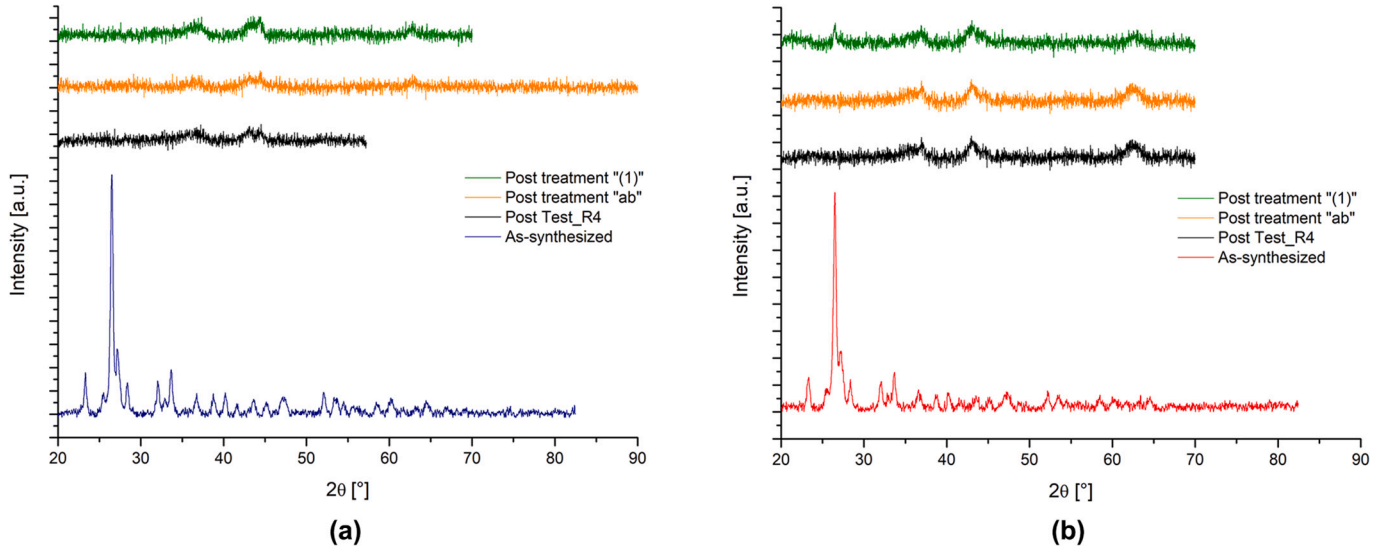

Fig. 8. XRD analyses of NiCoMo (a) and ZnCoMo (b) catalysts in as-synthesized form, after treatment "*(1)*", after treatment "*ab*",and after recycling test (*Test_R4*).

uniform distribution. The good performance of amorphous materials does not occur only for DO of vegetable oils: according to Wang et al. [75], who studied amorphous Co-Mo-B applied to hydrodeoxygenation of bio-oils, the disordered arrangement exposes more active sites to the reactants, enhancing their availability for the hydrodeoxygenation. On the other hand, the hypothesis of very low-sized crystallites would imply the formation of several new crystalline borders with a higher exposition of unsaturated metallic active sites.

4. Conclusions

In this study, NiCoMo and ZnCoMo catalysts reported in the literature were successfully re-synthesized, as verified through Fourier-transform infrared spectroscopy, X-ray diffraction, pore analyses, and temperature programmed reduction.

NiCoMo and ZnCoMo catalysts were successfully repurposed from propane oxidative-dehydrogenation to deoxygenation reaction for green diesel production, with satisfying performances in the whole domain of tested conditions (280–320 °C, 4–10 $\%_{w/w}$ catalyst-to-oil ratio, and 2–6 h of reaction time), except for the combination 280 °C, 4 $\%_{w/w}$, 2 h.

The catalysts exhibited encouraging performance stability over recycling tests (four cycles), keeping complete conversions of triglycerides and high diesel yields up to four successive deoxygenation cycles. This confirmed the successful repurposing. However, a higher number of cycles may constitute a more robust proof-of-concept for industrial-scale continuous operations.

ZnCoMo could be slightly more promising than NiCoMo because it showed hints of higher catalytic activity (related to higher acidity) and elemental stability in cyclic usage.

The unreplicated 2^3 factorial DoE with replications at the center point worked satisfactorily for the explorative purposes of this work. Still, this choice limited the regressions of surface responses to the form of "first-order main-effects model with interactions": this form was deemed to fit for DO performance parameters, but not for deep details of product compositions.

Future work could focus on the use of more complex design of experiments, in view of industrial scale-up studies, that may need to identify all main potential sources of costs or effectiveness improvement. For instance, a fractional design of experiments with replicated runs at factorial points may be more suitable for industrial scale-up purposes; the factors to be investigated by this design could include one or more "held-constant factors" of this work (mixing, solvent-to-oil mass ratio, catalyst activation procedure, quantity of loaded H_2 for DO). Another option could be the search for quadratic forms in response surfaces, suitable for the study of product composition, as well as for optimization purposes; central composite designs could work for this, e.g., allowing searching for satisfying deoxygenation working points at lowered temperatures, oil-to-catalyst-ratios, and reaction durations: lower levels of those factors for sure can improve DO sustainability and limit their negative interactions. These future studies by empowered design of experiments, up to optimizations of process parameters, may assist the repurposing of NiCoMo and ZnCoMo catalysts into the development of DO processes from the laboratory-scale batch reactor of this work to industrial-scale continuous process of green diesel production: proposed empirical modelling may help in cost analysis and optimization, as well as assist in the needed intermediate-scale studies such as fluid-dynamic mock-ups or pilots for continuous production.

Funding

The research leading to this work was funded by the RIA2023 (Ricerca di Interesse di Ateneo 2023) research project *"Produzione catalitica di green diesel di I, II o III generazione tramite conversione di oli di origine biologica"* (Scientific Manager – Andrea Di Giuliano) with funds provided by Università degli Studi dell'Aquila - Department of Industrial and Information Engineering and Economics (DIIIE).

CRediT authorship contribution statement

S. Lucantonio: Writing – review & editing, Writing – original draft, Visualization, Software, Investigation, Formal analysis, Data curation. **G. Di Vito Nolfi:** Resources, Methodology, Investigation, Data curation. **C. Courson:** Writing – review & editing, Visualization, Validation, Software, Resources, Methodology, Investigation, Formal analysis, Data curation, Conceptualization. **K. Gallucci:** Writing – review & editing, Visualization, Validation, Supervision, Resources, Project administration, Methodology, Formal analysis, Data curation, Conceptualization. **A. Di Giuliano:** Writing – review & editing, Writing – original draft, Visualization, Validation, Supervision, Software, Resources, Project administration, Methodology, Funding acquisition, Formal analysis, Data curation, Conceptualization. **L. Rossi:** Writing – review & editing, Visualization, Validation, Supervision, Resources, Project administration, Methodology, Formal analysis, Data curation, Conceptualization.

Declaration of competing interest

The authors declare that they have no known competing financial interests or personal relationships that could have appeared to influence the work reported in this paper.

Data availability

Data will be made available on request.

Acknowledgment

The authors thank Ing. Dipl. Giampaolo Antonelli for the technical support with PSD analyses, Dott. Lorenzo Arrizza for assistance with SEM-EDS analyses and Dr. Martina Foschi for her help with ICP-MS analyses.

Appendix A. Supplementary data

Supplementary data to this article can be found online at https://doi.org/10.1016/j.fuproc.2024.108173.

References

[1] The Paris Agreement, Available from, https://unfccc.int/process-and-meetings/the-paris-agreement.
[2] UN Climate Change Conference - United Arab Emirates [cited 2024 03/06]. Available from: https://unfccc.int/cop28.
[3] P. Achakulwisut, et al., Global fossil fuel reduction pathways under different climate mitigation strategies and ambitions, Nat. Commun. 14 (1) (2023) 5425.
[4] Sixth Assessment Report [cited, Available from: https://www.ipcc.ch/assessment-report/ar6/, 2024 09–09.
[5] R. Estevez, et al., Internal Combustion Engines and Carbon-Neutral Fuels: a Perspective on Emission Neutrality in the European Union, Energies 17 (5) (2024) 1172.
[6] A.Z. Aklilu, Gasoline and diesel demand in the EU: Implications for the 2030 emission goal, Renew. Sust. Energ. Rev. 118 (2020) 109530.
[7] S.V. Sagin, et al., Use of biofuels in marine diesel engines for sustainable and safe maritime transport, Renew. Energy 224 (2024) 120221.
[8] Suez blockage is holding up $9.6bn of goods a day [cited 2024 09–09]Available from: https://web.archive.org/web/20210326024224/https://www.bbc.com/news/business-56533250.
[9] Diesel Fuel Market Size, Share and Global Trend by End-Use (Cars, Trucks, Military Vehicles, Heavy Off-Road Vehicles, Ships, Generators, others) and Regional Forecast, 2024–2032, Available from: https://www.fortunebusinessinsights.com/industry-reports/diesel-fuel-market-101317.
[10] Incentivi alla mobilità a zero emissioni: l'UE finanzia 42 progetti per oltre 424 milioni di €, Available from, https://italy.representation.ec.europa.eu/notizie-ed-eventi/notizie/incentivi-alla-mobilita-zero-emissioni-lue-finanzia-42-progetti-oltre-424-milioni-di-eu-2024-04-10_it.
[11] O. Chiavola, E. Recco, Emission Performance of a Diesel Engine Fuelled with Petrol Diesel, Green Diesel, and Waste Cooking Oil Blends, J. Comb. 2018 (2018).
[12] S.L. Douvartzides, et al., Green Diesel: Biomass Feedstocks, production Technologies, Catalytic Research, fuel Properties and Performance in Compression Ignition Internal Combustion Engines, Energies 12 (5) (2019).

[13] S. Lucantonio, et al., Green Diesel Production via Deoxygenation Process: a Review, Energies 16 (2) (2023).
[14] T.N. Kalnes, et al., A Technoeconomic and Environmental Life Cycle Comparison of Green Diesel to biodiesel and Syndiesel, Environ. Prog. Sustain. Energy 28 (1) (2009) 111–120.
[15] G. Di Vito Nolfi, K. Gallucci, L. Rossi, Green Diesel Production by Catalytic Hydrodeoxygenation of vegetables oils, Int. J. Environ. Res. Public Health 18 (24) (2021).
[16] N. Aliana-Nasharuddin, et al., Production of green diesel from catalytic deoxygenation of chicken fat oil over a series binary metal oxide-supported MWCNTs, RSC Adv. 10 (2) (2020) 626–642.
[17] H.D. Almeida, et al., Diesel-like hydrocarbon fuels by catalytic cracking of fat, oils, and grease (FOG) from grease traps, J. Energy Inst. 90 (3) (2017) 337–354.
[18] C.A. Scaldaferri, V.M.D. Pasa, Hydrogen-free process to convert lipids into bio-jet fuel and green diesel over niobium phosphate catalyst in one-step, Chem. Eng. J. 370 (2019) 98–109.
[19] S.T. Mohammed, et al., Evaluation and optimal design of a high stability hydrothermal deoxygenation process for production of green diesel fuel via deoxygenation of waste cooking oil, Process. Saf. Environ. Prot. 159 (2022) 489–499.
[20] S.T. Mohammed, et al., Enhancement of stability of Pd/AC deoxygenation catalyst for hydrothermal production of green diesel fuel from waste cooking oil, Chem. Eng. Sci. 251 (2022).
[21] N.A.A. Razak, et al., Production of green diesel via hydrogen-free and solventless deoxygenation reaction of waste cooking oil, J. Clean. Prod. 366 (2022).
[22] I. Vazquez-Garrido, et al., Synthesis of NiMo catalysts supported on Mn-Al₂O₃ for obtaining green diesel from waste soybean oil, Catal. Today 365 (2021) 327–340.
[23] M. Herskowitz, et al., A commercially-viable, one-step process for production of green diesel from soybean oil on Pt/SAPO-11, Fuel 111 (2013) 157–164.
[24] H. Jahromi, et al., Production of green transportation fuels from Brassica carinata oil: a comparative study of noble and transition metal catalysts, Fuel Process. Technol. 215 (2021).
[25] K.W. Jeon, et al., Deoxygenation of non-edible fatty acid for green diesel production: effect of metal loading amount over Ni/MgO-Al₂O₃ on the catalytic performance and reaction pathway, Fuel 311 (2022).
[26] P. Lovás, et al., Conversion of rapeseed oil via catalytic cracking: effect of the ZSM-5 catalyst on the deoxygenation process, Fuel Process. Technol. 134 (2015) 223–230.
[27] G. Petropoulos, et al., Transformation of vegetable oils into green diesel over Ni-Mo catalysts supported on titania, Catal. Today 423 (2023).
[28] M.J.A. Romero, et al., Deoxygenation of waste cooking oil and non-edible oil for the production of liquid hydrocarbon biofuels, Waste Manag. 47 (2016) 62–68.
[29] A.S. Zamani, M. Saidi, A.T. Najafabadi, Selective production of diesel-like alkanes via Neem seed oil hydrodeoxygenation over Ni/MgSiO3 catalyst, Renew. Energy 209 (2023) 462–470.
[30] N. Asikin-Mijan, et al., Production of green diesel via cleaner catalytic deoxygenation of Jatropha curcas oil, J. Clean. Prod. 167 (2017) 1048–1059.
[31] A.I. Tsiotsias, et al., Selective catalytic deoxygenation of palm oil to produce green diesel over Ni catalysts supported on ZrO2 and CeO2-ZrO2: Experimental and process simulation modelling studies, Renew. Energy 206 (2023) 582–596.
[32] K. Kandel, et al., Supported iron nanoparticles for the hydrodeoxygenation of microalgal oil to green diesel, J. Catal. 314 (2014) 142–148.
[33] B.X. Peng, et al., Towards Quantitative Conversion of Microalgae Oil to Diesel-Range Alkanes with Bifunctional Catalysts, Angewandte Chemie-Int. Ed. 51 (9) (2012) 2072–2075.
[34] W.J. Song, C. Zhao, J.A. Lercher, Importance of Size and distribution of Ni Nanoparticles for the Hydrodeoxygenation of Microalgae Oil, Chem. Eur. J. 19 (30) (2013) 9833–9842.
[35] L. Zhou, A. Lawal, Evaluation of Presulfided NiMo/γ-Al₂O₃ for Hydrodeoxygenation of Microalgae Oil to produce Green Diesel, Energy Fuel 29 (1) (2015) 262–272.
[36] R. Estevez, et al., Internal Combustion Engines and Carbon-Neutral Fuels: a Perspective on Emission Neutrality in the European Union, Energies 17 (2024), 10.3390/en17051172.
[37] S. Dell'Aversano, et al., E-Fuels: A Comprehensive Review of the Most Promising Technological Alternatives towards an Energy Transition, Energies 17 (16) (2024) 3995.
[38] D. Lin, et al., Kinetic insights into deoxygenation of vegetable oils to produce second-generation biodiesel, Fuel 333 (2023).
[39] D. Lin, et al., Catalyst Design strategies for Deoxygenation of Vegetable oils to produce Second-Generation biodiesel, Ind. Eng. Chem. Res. 62 (32) (2023) 12462–12481.
[40] A. Srifa, et al., Production of bio-hydrogenated diesel by catalytic hydrotreating of palm oil over NiMoS2/gamma-Al2O3 catalyst, Bioresour. Technol. 158 (2014) 81–90.
[41] T.V. Choudhary, C.B. Phillips, Renewable fuels via catalytic hydrodeoxygenation, Appl. Catal. a-General 397 (1–2) (2011) 1–12.
[42] R. Kaewmeesri, et al., Deoxygenation of Waste Chicken Fats to Green Diesel over Ni/Al2O3: effect of Water and Free Fatty Acid Content, Energy Fuel 29 (2) (2015) 833–840.
[43] M.Y. Choo, et al., Deoxygenation of triolein to green diesel in the H-2-free condition: effect of transition metal oxide supported on zeolite Y, J. Anal. Appl. Pyrolysis 147 (2020).
[44] S.R. Naqvi, et al., Recent progress in catalytic deoxygenation of biomass pyrolysis oil using microporous zeolites for green fuels production, Fuel 333 (2023).
[45] N. Arun, R.V. Sharma, A.K. Dalai, Green diesel synthesis by hydrodeoxygenation of bio-based feedstocks: strategies for catalyst design and development, Renew. Sust. Energ. Rev. 48 (2015) 240–255.
[46] S. Chen, G.L. Zhou, C.X. Miao, Green and renewable bio-diesel produce from oil hydrodeoxygenation: strategies for catalyst development and mechanism, Renew. Sustain. Energy Rev. 101 (2019) 568–589.
[47] H. Zhu, et al., Ni-Fe-Al LDH derived NiFe nanosheet for green diesel production from lipid hydrotreatment, Fuel Process. Technol. 239 (2023) 107537.
[48] S. Arias, et al., Hydrogen-free deoxygenation of industrial vegetable oil waste using Ce, Zr-NiAl catalysts for second-generation biofuels production, Mol. Catal. 529 (2022) 112554.
[49] Z. Zhang, et al., LDH derived Co-Al nanosheet for lipid hydrotreatment to produce green diesel, Fuel 333 (2023) 126341.
[50] J. Velasquez, et al., Propane Oxidative Dehydrogenation on ZnCoMo and NiCoMo Catalysts Obtained from ϕy and ϕx Precursors, Ind. Eng. Chem. Res. 52 (16) (2013) 5582–5586.
[51] F. Cavani, N. Ballarini, A. Cericola, Oxidative dehydrogenation of ethane and propane: how far from commercial implementation? Catal. Today 127 (1–4) (2007) 113–131.
[52] H. Liu, et al., Catalysts development for O2-assisted oxidative dehydrogenation of propane to propylene, Chem. Commun. 60 (2024) 7535–7554, https://doi.org/10.1039/D4CC01948B.
[53] Y. Gambo, et al., Catalyst design and tuning for oxidative dehydrogenation of propane – a review, Appl. Catal. A Gen. 609 (2021) 117914.
[54] Fatty acids in oils and fats. Preparation of methyl esters boron trifluoride method, 1997 [cited 2023 14/09].
[55] M. Ameen, et al., Catalytic hydrodeoxygenation of rubber seed oil over sonochemically synthesized Ni-Mo/γ-Al₂O₃ catalyst for green diesel production, Ultrason. Sonochem. 51 (2019) 90–102.
[56] A. Kaewchada, et al., Production of bio-hydrogenated diesel from palm oil using Rh/HZSM-5 in a continuous mini fixed-bed reactor, Chem. Eng. Process. Process Intensification (2021) 168.
[57] M. Ruangudomsakul, et al., Hydrodeoxygenation of palm oil to green diesel products on mixed-phase nickel phosphides. Molecular, Catalysis (2022) 523.
[58] A. Sonthalia, N. Kumar, Hydroprocessed vegetable oil as a fuel for transportation sector: a review, J. Energy Inst. 92 (1) (2019) 1–17.
[59] D.C. Montgomery, Design and Analysis of Experiments, John wiley & sons, 2017.
[60] M. Thommes, et al., Physisorption of gases, with special reference to the evaluation of surface area and pore size distribution (IUPAC Technical Report), Pure Appl. Chem. 87 (9–10) (2015) 1051–1069.
[61] M.L. Shozi, et al., An investigation of Cu-Re-ZnO catalysts for the hydrogenolysis of glycerol under continuous flow conditions, Sustainable Energy Fuels 1 (6) (2017) 1437–1445.
[62] J.L. Brito, A.L. Barbosa, Effect of phase composition of the oxidic precursor on the HDS activity of the sulfided molybdates of Fe(II), Co(II), and Ni(II), J. Catal. 171 (2) (1997) 467–475.
[63] J. Duan, et al., Diesel-like hydrocarbons obtained by direct hydrodeoxygenation of sunflower oil over Pd/Al-SBA-15 catalysts, Catal. Commun. 17 (2012) 76–80.
[64] F.P. Sousa, et al., Simultaneous deoxygenation, cracking and isomerization of palm kernel oil and palm olein over beta zeolite to produce biogasoline, green diesel and biojet-fuel, Fuel 223 (2018) 149–156.
[65] W. Szeto, D.Y.C. Leung, Is hydrotreated vegetable oil a superior substitute for fossil diesel? A comprehensive review on physicochemical properties, engine performance and emissions, Fuel 327 (2022).
[66] N. Hongloi, et al., Nickel catalyst with different supports for green diesel production, Energy 182 (2019) 306–320.
[67] E. Kordouli, et al., Mo promoted Ni-Al2O3 co-precipitated catalysts for green diesel production, Appl. Catal. B Environ. 229 (2018) 139–154.
[68] S. Lycourghiotis, et al., Transformation of residual fatty raw materials into third generation green diesel over a nickel catalyst supported on mineral palygorskite, Renew. Energy 180 (2021) 773–786.
[69] F. Jamil, et al., Phoenix Dactylifera Kernel Oil used as potential source for Synthesizing Jet fuel and Green Diesel, Energy Procedia 118 (2017) 35–39.
[70] Y. Sugami, E. Minami, S. Saka, Hydrocarbon production from coconut oil by hydrolysis coupled with hydrogenation and subsequent decarboxylation, Fuel 197 (2017) 272–276.
[71] M. Krár, et al., Fuel purpose hydrotreating of sunflower oil on CoMo/Al2O3 catalyst, Bioresour. Technol. 101 (23) (2010) 9287–9293.
[72] S.K. Kim, et al., Production of renewable diesel by hydrotreatment of soybean oil: effect of reaction parameters, Chem. Eng. J. 228 (2013) 114–123.
[73] L. Zhou, A. Lawal, Hydrodeoxygenation of microalgae oil to green diesel over Pt, Rh and presulfided NiMo catalysts, Cat. Sci. Technol. 6 (5) (2016) 1442–1454.
[74] P. Aiamsiri, et al., Biohydrogenated Diesel from Palm Oil Deoxygenation over Unsupported and gamma-Al2O3 Supported Ni-Mo Catalysts, Energy Fuel 35 (18) (2021) 14793–14804.
[75] W. Wang, et al., Amorphous Co–Mo–B catalyst with high activity for the hydrodeoxygenation of bio-oil, Catal. Commun. 12 (6) (2011) 436–440.